sustainability

MDPI

Article

Proposal and Comprehensive Analysis of a Novel Combined Plant with Gas Turbine and Organic Flash Cycles: An Application of Multi-Objective Optimization

Ramin Ghiami Sardroud [1,*], Amirreza Javaherian [2,*], Seyed Mohammad Seyed Mahmoudi [2], Mehri Akbari Kordlar [3] and Marc A. Rosen [4]

1 Faculty of Mechanical Engineering, Sahand University of Technology, Tabriz P.O. Box 51335, Iran
2 Department of Mechanical Engineering, Faculty of Mechanical Engineering, University of Tabriz, Tabriz P.O. Box 51368, Iran
3 Center of Energy Technology (ZET), University of Bayreuth, 95445 Bayreuth, Germany; mehri.ak1366@gmail.com
4 Faculty of Engineering and Applied Science, University of Ontario Institute of Technology, Oshawa, ON L1G 0C5, Canada; marc.rosen@ontariotechu.ca
* Correspondence: ram.ghiami@gmail.com (R.G.S.); a_javaherian@tabrizu.ac.ir (A.J.)

Abstract: Environmental, exergo-economic, and thermodynamic viewpoints are thoroughly investigated for a state-of-the-art hybrid gas turbine system and organic flash cycle. For the proposed system, the organic flash cycle utilizes the waste thermal energy of the gases exiting the gas turbine sub-system to generate additional electrical power. Six distinct working fluids are considered for the organic flash cycle: R245fa, n-nonane, n-octane, n-heptane, n-hexane, and n-pentane. A parametric investigation is applied on the proposed combined system to evaluate the impacts of seven decision parameters on the following key operational variables: levelized total emission, total cost rate, and exergy efficiency. Also, a multi-objective optimization is performed on the proposed system, taking into account the mentioned three performance parameters to determine optimum operational conditions. The results of the multi-objective optimization of the system indicate that the levelized total emission, total cost rate, and exergy efficiency are 74,569 kg/kW, 6873 $/h, and 55%, respectively. These results also indicate the improvements of 16.45%, 6.59%, and 3% from the environmental, economic, and exergy viewpoints, respectively. The findings reveal that utilizing n-nonane as the working fluid in the organic flash cycle can yield the lowest levelized total emission, the lowest total cost rate, and the highest exergy efficiency.

Keywords: gas turbine; organic flash cycle; exergo-economic analysis; optimization; levelized total emission

check for updates

Citation: Ghiami Sardroud, R.; Javaherian, A.; Seyed Mahmoudi, S.M.; Akbari Kordlar, M.; Rosen, M.A. Proposal and Comprehensive Analysis of a Novel Combined Plant with Gas Turbine and Organic Flash Cycles: An Application of Multi-Objective Optimization. *Sustainability* **2023**, *15*, 14152. https://doi.org/10.3390/su151914152

Academic Editors: Luigi Grossi and Marina Bertolini

Received: 8 August 2023
Revised: 16 September 2023
Accepted: 20 September 2023
Published: 25 September 2023

1. Introduction

Considering that the global need for energy is increasing, researchers are seeking strategies to utilize less energy and prevent the negative effects of burning fossil fuels such as environmental pollution and global warming. It is desired that options provide energy conversion with improved efficiency and lower carbon emissions. Fossil fuels, due to their availability and convenience in utilization compared to other energy sources, are receiving a great deal of attention [1]. Fossil fuels have a key disadvantage. By using the fossil fuels, the environmental consequences such as global warming, subsequent climate changes, and air pollution increase [2]. In order to limit these impacts, two approaches can be considered: utilizing renewable and/or sustainable energy sources (e.g., hydro, biomass, solar, geothermal, and wind energies) and the waste heat recovery (WHR) of exhaust gases from the topping cycles, along with other efficiency improvement measures. Renewable and sustainable energy sources usually provide energy services with practically no air pollution and greenhouse gas emissions [3]. However, these energy sources have

some limitations, such as cost concerns for hydropower and solar energies and location dependence for geothermal energy [4]. The use of WHR not only lowers the use of fossil fuels but additionally boosts the overall efficiency of the system and lessens environmental problems [5].

The WHR approach forms the foundation of the combined plant proposed in the current study. The system comprises two integrated cycles operating at various temperatures. After converting a portion of high-temperature thermal energy to electricity, the topping cycle transforms the rest of the high-temperature energy to the low-temperature cycle. In the bottoming cycle, a share of this thermal energy is transformed into electricity, while the remainder is discharged to the atmosphere [6,7]. Since electricity is produced by two components in the combined cycle, applying WHR can boost the efficiency of the overall system [8].

Among various systems, the gas turbine (GT) system is potentially suitable as a topping cycle due to being cost-effective, efficient, and being able to use a wide range of hydrocarbon fuels [9,10]. However, without WHR, about 60% of the energy in a typical GT is rejected into the atmosphere at high temperature [11,12]. Using the advanced gas turbine in the hybrid system results in an enhanced energy efficiency of 50–58% [13]. As a result, the efficiency of the entire plant can be improved by integrating the bottoming cycle with the GT system. Much effort has been committed to boost the efficiencies of the conventional GT cycles. Among these is CGAM cogeneration system, which integrates a gas turbine with a heat recovery steam generator (HRSG) and an air preheater [14–16]. The utilization of air preheater boosts the efficiencies based on exergy and energy of the system, as the air passing into the combustion chamber absorbs heat from the hot gases leaving the turbine, which lowers fuel consumption. It is potentially advantageous to use this type of heat exchanger when the temperature of the air entering the combustion chamber is less than the temperature of the gases exiting the turbine; otherwise, the efficiency of the system can drop. The GT cycle is most extensively employed in the aviation [17–19] and maritime industries [20].

Exergo-economic and exergy evaluations of the GT cycle have been performed by Ameri and Enadi [21]. They concluded that the combustion chamber has the highest exergy destruction rate, and this variable is reduced by raising the chamber's entrance temperature. In addition, as the intake temperature of the gas turbine climbs from 1100 K to about 1450 K, the cost of destroyed exergy is lowered by 22%. To increase the efficiency of the GT cycle, Pirkandi et al. [22] employed solar energy in the cycle. This procedure increased the temperature of the air passing into the chamber, decreasing the amount of fuel used. Overall, 10% more power is generated by the solar GT cycle than the traditional system. Avval et al. [23] investigated the GT cycle with a preheater from economic, energy, exergy, and environmental perspectives. By utilizing an evolutionary method, the system was subjected to a multi-objective optimization (MOO). The authors also evaluated the impacts of pressure ratio in the compressor and gas turbine isentropic efficiencies, and combustion chamber intake temperature on the environmental, economic, and thermodynamic performances of the plant.

Altinkaynak and Ozturk [24] analyzed an integrated cycle including gas turbine, as well as supercritical carbon dioxide (S-CO_2), trans-critical carbon dioxide, and ORC systems, to generate thermal energy, cooling, electricity, and hydrogen. The exergy and energy efficiencies of the multi-generation plant have been found to be 42.0% and 44.7%, respectively. Maroufi et al. [25] compared the performances of direct combination systems, including GT and pressurized fuel cell and GT and atmospheric fuel cell, and indirect combination systems, from energy and economic standpoints. The direct combined GT cycle and pressurized fuel cell were found to offer the best thermodynamic and economic characteristics. An innovative water and electricity generation system that utilized the waste heat of the GT cycle was examined thermodynamically, economically, and environmentally by Liu et al. [26]. This system included a Kalina cycle, a GT cycle, and a desalination unit. Under basic design conditions, the overall products' cost, the capacity of freshwater generation, the levelized total emission (LTE), and the exergy efficiency were found to be

20.2 $/GJ, 10.8 kg/s, 63.7 kg/W, and 43.1%, respectively. Also, the combustion chamber had the greatest exergy destruction rate among the components of the proposed system. Du et al. [27] investigated the economic, exergy, and energy performances of supercritical and trans-critical carbon dioxide cycles driven by a GT system. The plant's exergy and energy efficiencies were found to be 46.1% and 24.9%, respectively. Additionally, the total cost rate of investment and the products unit exergy cost were 126.1 $/h and 6.31 $/GJ, respectively.

Several systems have been suggested for their use as a low-temperature cycle in hybrid gas turbine-based plants. A steam Rankine cycle has been often used as the low-temperature cycle for a GT system. However, steam Rankine cycle has some significant disadvantages. This cycle utilizes water as the working fluid, and it is necessary to superheat water before inputting it to the turbine. Otherwise, there is the potential for erosion of turbine blades, and utilization of expensive and complex turbines [28]. To overcome these challenges, organic working fluids are proposed as alternatives. An organic fluid typically has a critical pressure and temperature and molecular mass higher than water [1,28]. One of the main cycles in the WHR field is the ORC. This system utilizes an organic working fluid and avoids many of the issues of the steam Rankine cycle. Due to the simplicity, reliability, and adaptability of the ORC, it has recently attracted a great deal of research interest [29,30]. The major drawback with this cycle is that the evaporation process occurs at an unchanged temperature, which leads to a pinch point problem. This difficulty is caused by the lack of sufficient temperature compatibility between the two fluid flows during heat transfer, which lowers the exergy efficiency and causes notable exergy destruction in heat exchangers.

Khaljani et al. [31] investigated a combined plant with ORC and GT sub-systems from environmental, economic, and thermodynamic perspectives. They concluded that in the combustion chamber, exergy was destroyed at the greatest rate. They also highlighted how the exergy and energy efficiencies of the plant rise with the compressor pressure ratio and isentropic efficiencies of the compressor and turbine. Nevertheless, the rise in these parameters increased the overall cost rate. Therefore, there should be an optimal value for these three specified parameters, where the efficiencies are at the highest values and the overall cost rate is at the lowest value. The desired values for the compressor and the turbine isentropic efficiencies and compressor pressure ratio were 87%, 89%, and 13.8, respectively. Ahmadi et al. [1] examined the integration of a GT cycle and an ORC from energy and exergy viewpoints. In this research, six working fluids were employed in the ORC to determine which is the most suitable. Based on the exergy and energy efficiencies, dimethyl carbonate and o-xylene were seen to exhibit the best and the worst performances, respectively. The authors also investigated the impacts of operating pressure of the ORC on the exergy and energy efficiencies. The outcomes showed that the best optimal value for this variable to maximize the energy and exergy efficiencies is the highest accessible pressure reported in this research for each working fluid. Mohammadi et al. [32] thermodynamically analyzed an absorption refrigeration cycle, ORC, and combined GT cycle. This integrated system was capable of providing 8 kW of cooling and 30 kW of power under specified conditions. Parametric investigation revealed that the pressure ratio and inlet temperature of the turbine are the two variables that most affect the performance of the system. Cao et al. [33] comprehensively evaluated the integration of a GT system and an ORC from thermodynamic perspective. They compared the GT-Rankine integrated system and the GT-ORC integrated plant, and the findings demonstrated that the GT-ORC integrated plant possesses superior thermodynamic performance. Three distinct ORC working fluids were employed, and the optimum performance of the GT-ORC was obtained when toluene was utilized. A trigeneration system combining the GT cycle, single-effect chiller, water heater, and ORC was evaluated by Ahmadi et al. [34] based on exergo-environmental analysis. With regard to the exergy efficiency and carbon dioxide emission, this system exhibited superior performance over the GT combined cycles for the specified input data. The authors also clearly highlighted that the environmental and thermodynamic performances of this system are notably affected by the isentropic efficiency of the gas turbine, the gas turbine inlet temperature, and the compressor pressure ratio.

Hemdari and Subbarao [35] analyzed a combined GT and reheat ORC from energy and exergy perspectives. In this research, they investigated hexane, benzene, and cyclopentane as viable working fluids for the ORC. They reported that the maximum output power of cycle is obtained when benzene is employed. Sun et al. [36] investigated the combined S-CO_2 cycle and ORCs for WHR application of a GT from exergo-economic and thermodynamic standpoints. The combined plant consisted of two S-CO_2 cycles and one ORC. The exergy and energy efficiencies and the exergo-economic factor of the proposed plant were found to be 51.9%, 48.6%, and 28.3%, respectively. The performances of the S-CO_2 cycle and the ORC were compared for waste recovery of a GT-sub system by Ancona et. al. [37]. They observed that when the same installed topping GT cycle is utilized for both S-CO_2 and ORC sub-systems, the S-CO_2 cycle exhibits greater energy efficiency than the ORC. Pan et al. [38] considered recompression, reheat, and pressurized intercooling supercritical CO_2-ORC for WHR from a GT. They assessed and optimized the suggested system from economic, energy, exergy, and environmental viewpoints. They reported values for the system of 84.5%, 66.9%, and 41.2%, respectively, for its environmental, exergy, and energy efficiencies.

Another significant system in the field of WHR is the Kalina cycle, which, due to utilizing zeotropic mixtures, can address the temperature mismatch problem between high- and low-temperature working fluids. As indicated before, temperature profile mismatching is one of the major challenges for ORCs. However, the Kalina cycle's configuration complexity has motivated researchers to focus on the thermodynamic analysis of this system [39]. A new cogeneration cycle made up of a GT cycle, the Kalina cycle, and a freshwater production unit was proposed by Ding et al. [40]. They evaluated this system from environmental, economic, and thermodynamic viewpoints. They also employed MOO to obtain the most effective operational variables. The greatest exergy efficiency and the lowest levelized total emission were observed to be 43.8% and 62.6 kg/W, respectively. Zhang et al. [41] considered the Kalina cycle as the low-temperature source to reuse the waste heat of a GT system, and assessed the plant from thermodynamic and environmental perspectives. Referring to the thermodynamic optimization findings, the exergy and energy efficiencies of the system were found to be 47.2% and 46.1%, respectively, and LTE was 60.1 kg/W. The combustion chamber was observed to be responsible for the greatest rate of exergy destruction in the system. Ebrahimi-Moghadam et al. [42] comprehensively studied a combined plant containing GT system and Kalina cycle considering environmental, economic, exergy, and energy assessments. The system's main operational performance parameters, including the exergy and energy efficiencies, LTE, and levelized total cost (LTC), were treated as the objective functions. Based on design parameters, energy and exergy efficiencies, LTE and LTC were found to be 69.4%, 37.9%, 88.0 kg/W, and 8.96 $/W, respectively. Köse et al. [2] considered the Rankine and Kalina sub-systems as the low-temperature cycles to utilize waste heat from a GT plant. They conducted energy, exergy, economic, and environmental evaluations for the suggested system. Considering the GT and Rankine cycle (RC), the first law efficiency was 41.7%, but the energy efficiency of the GT-RC-Kalina system was 46.4%.

Ji-chao and Sobhani [43] thermodynamically and exergo-economically evaluated a cogeneration system including GT, supercritical CO_2, and Kalina cycles. This system exhibited exergy and energy efficiencies of 41.0% and 78.2%, respectively. The net present value and the payback period were calculated as 5.37×10^6 $ and 6.9 years, respectively. Ebrahimi-Moghadam [44] investigated a trigeneration system, including GT, Kalina, and ejector cycles, from exergo-environmental and exergo-economic perspectives. Based on the optimization results, the exergo-economic criterion, the exergo-environmental criterion, and the exergy efficiency were observed as 58.4 $/GJ, 42.7 kg/GJ, and 30.8%, respectively. Environmental, economic, exergy, and energy performances of an integrated micro-GT cycle and a superheated Kalina cycle were analyzed and optimized by Liu and Ehyaei [45]. This system exhibited exergy and energy efficiencies of 50.8% and 51.7%, respectively. Moreover, the greatest exergy destruction was attributable to the gasifier. Employing

the superheated Kalina cycle as the bottoming cycle decreased the payback period from 9.07 years to 4.6 years.

As indicated previously, an important disadvantage of the ORC is the temperature mismatch between the working fluid and heat source throughout the process of heat transfer, resulting in a rise in irreversibility and a drop in exergy efficiency. To tackle this difficulty, researchers have presented several promising approaches, one of which is the trilateral flash cycle (TFC). Yari et al. [46] compared the thermo-economics of the Kalina cycle, ORC, and TFC utilizing a low-temperature heat source. The expander isentropic efficiency had a notable impact on the production cost of the TFC, even though TFC had greater net output power than the Kalina cycle and ORC. Based on references [47,48], the manufacturing of a highly efficient two-phase expander poses a substantial challenge for the TFC. The organic flash cycle (OFC) is well known as a developed version of the TFC. In addition to the fact that this cycle does not require a two-phase expander and can address the mentioned disadvantage of the TFC, it can also address the temperature profiles mismatch in the ORC. The above advantages suggest that the OFC is potentially one of the best options for utilizing GT cycles' waste heat.

Ho et al. [49] demonstrated that the energy efficiencies of the OFC and the optimized ORC for low-grade heat sources are the same. Moreover, aromatic hydrocarbons were reported as the most suitable working fluids to be utilized in OFCs and ORCs. Mondal and De [50] utilized R600-R245fa mixture as the OFC working fluid to reuse the waste heat of the flue gas devoid of SO_2. The GWP of this mixture is less than 800 kg of CO_2 per kg of fluid. This mixture can provide a higher output power for the OFC than that of the OFC utilizing pure working fluids. The thermodynamic and thermo-economic characteristics of four OFC systems using five distinct working fluids were compared by Nemati et al. [51]. A simple OFC was seen to have the highest and the lowest cost per unit of produced electricity and exergy efficiency, respectively. The exergy investigation demonstrated that the enhanced expander-OFC has the greatest performance. However, the dual flash OFC attained the greatest economic performance out of the three proposed configurations. The best exergo-economic and exergy performances of systems were obtained when toluene was utilized as the working fluid. An organic Rankine flash cycle (ORFC) integrates the trilateral cycle with the ORC. De Campos et al. [52] compared the ORFC with the OFC, demonstrating that the greatest exergy efficiency is attained for the ORFC at lower volume flow ratio of the two-phase expansion than the OFC. Moreover, the exergy and energy efficiencies of the ORFC were higher than those of the OFC when utilizing pentane as the working fluid. Economic, exergy, and energy assessments of an ORFC were evaluated by Wang et al. [53]. They determined that utilizing working fluids with higher critical temperatures offer improved energy efficiencies and lower power costs. Based on the optimization findings, the ORFC was able to perform thermodynamically better than the ORC and the OFC. Wu et al. [54] evaluated an OFC integrated with a S-CO_2 recompression Brayton cycle (SCRBC) thermodynamically and thermo-economically. In this system, the OFC was utilized as the bottoming cycle to reuse the SCRBC waste heat. The findings revealed that the product overall unit cost and the exergy efficiency of the SCRBC integrated with the OFC were, respectively, 3.75% lower than and 6.57% higher than those of the standalone SCRBC. Moreover, the SCRBC combined with the OFC exhibited better thermo-economic and thermodynamic performances compared to the SCRBC integrated with the ORC. The authors considered seven different OFC working fluids, and the findings illustrated that the best thermo-economic and thermodynamic performances were obtained with n-nonane. For enhancing the performance of the SCRBC, three distinct bottoming systems, including Kalina cycle, OFC, and ORC, were considered to reuse the SCRBC waste heat and evaluated from the viewpoints of thermo-economics and thermodynamics by Mahmoudi et al. [55]. The SCRBC/ORC and SCRB/Kalina cycles showed the greatest and the lowest exergy efficiencies, respectively, while the SCRBC/ORC exhibited the best thermo-economic performance. Ten distinct working fluids were em-

ployed for the OFC and the ORC. The best thermodynamic and economic performances were achieved with n-nonane and R134a for the OFC and ORC, respectively.

A S-CO_2 cycle combined with an OFC driven by hybrid geothermal and solar energies was introduced by Que et al. [56]. In this system, a solar tower provided thermal energy to the S-CO_2 cycle, while the OFC was powered by the S-CO_2 system's waste heat and geothermal energy. The authors investigated four different OFC working fluids and discovered that R245ca is the best choice from exergy and energy viewpoints. The system efficiencies of exergy and energy were found to be 33.4% and 26.0%, respectively. Ai et al. [57] compared thermodynamically a new combined cooling, heating, and power (CCHP) system comprising the solar system and the regenerative OFC to a CCHP-ST-ORC system. The ratio of primary energy, which was defined as the ratio of useful energy output to the primary energy input, and the exergy efficiency were found to be 53.1% and 38.7%, respectively. Moreover, the consumption of natural gas for the CCHP-ST-OFC system was 9% lower than that for the CCHP-ST-ORC system.

The integration of the GT cycle with the OFC can have several practical implications, offering potential benefits in terms of efficiency, flexibility, and environmental impact. Practical implications of this integration are:

1. Enhanced efficiency: The integration of a GT cycle with an OFC allows for the recovery of waste heat from the GT exhaust gases. This waste heat can be utilized to generate additional power through the OFC. By effectively capturing and utilizing this waste heat, the overall system efficiency can be significantly improved compared with standalone GT cycles.
2. Flexible power generation: The combined GT-OFC system offers increased flexibility in power generation. The GT cycle provides a reliable and responsive power generation option, while the OFC can be utilized during periods of lower power demand or as a peaking power source. This flexibility allows for better matching of power generation with varying demand patterns, improving system reliability and grid stability.
3. Fuel diversity and decentralized energy generation: The integration of GT and OFC technologies allows for the utilization of a wider range of fuels. Gas turbines are known for their fuel flexibility, being able to operate on natural gas, liquid fuels, or even alternative fuels such as biofuels. By integrating an OFC, the system can also utilize low-grade waste heat sources, such as geothermal or industrial waste heat, further diversifying the fuel sources and enabling decentralized energy generation.
4. Environmental benefits: The integration of an OFC with a GT cycle can contribute to lower greenhouse gas emissions. The increased efficiency of the combined cycle reduces the amount of fuel required per unit of electricity generated, leading to lower CO_2 emissions. Additionally, by utilizing waste heat that would otherwise be discharged into the environment, the system helps to reduce thermal pollution.
5. Combined heat and power (CHP) applications: The integrated GT-OFC system is well-suited for combined heat and power applications. The waste heat recovered from the GT cycle can be utilized for combined electricity and thermal energy generation, providing simultaneous power and heat for industrial purposes, commercial buildings, or district heating systems. This CHP configuration improves overall energy efficiency and reduces primary energy consumption.

To our best knowledge, a complete examination via environmental, exergy, energy, and economic evaluations of a novel combined GT cycle with the OFC has not yet been conducted, which is the novelty of the current work. Moreover, another novelty of the paper is carrying out genetic algorithm-based multi-objective optimization. In addition, one of the most important aspects of this study is applying environmental analysis to the combined GT-OFC system. The present study aims to enhance the environmental, economic, and thermodynamic performances of the GT cycle by using an OFC to utilize GT waste heat. Parametric investigations are applied to evaluate the impacts of several factors on the LTE, total cost rate, and the exergy efficiency of the system. Single- and multi-objective optimizations were carried out to the GT cycle combined with the OFC to determine the lowest

total cost rate and LTE of the system and the highest exergy efficiency. In addition, six organic working fluids are examined, and the most appropriate working fluid is selected from environmental, economic, and thermodynamic viewpoints.

2. System Layout Description and Assumptions

Figure 1 depicts the proposed novel combined GT-OFC plant. The configuration includes a GT system as the topping cycle and an OFC as the bottoming cycle. In this hybrid system, the OFC uses the GT system's waste heat.

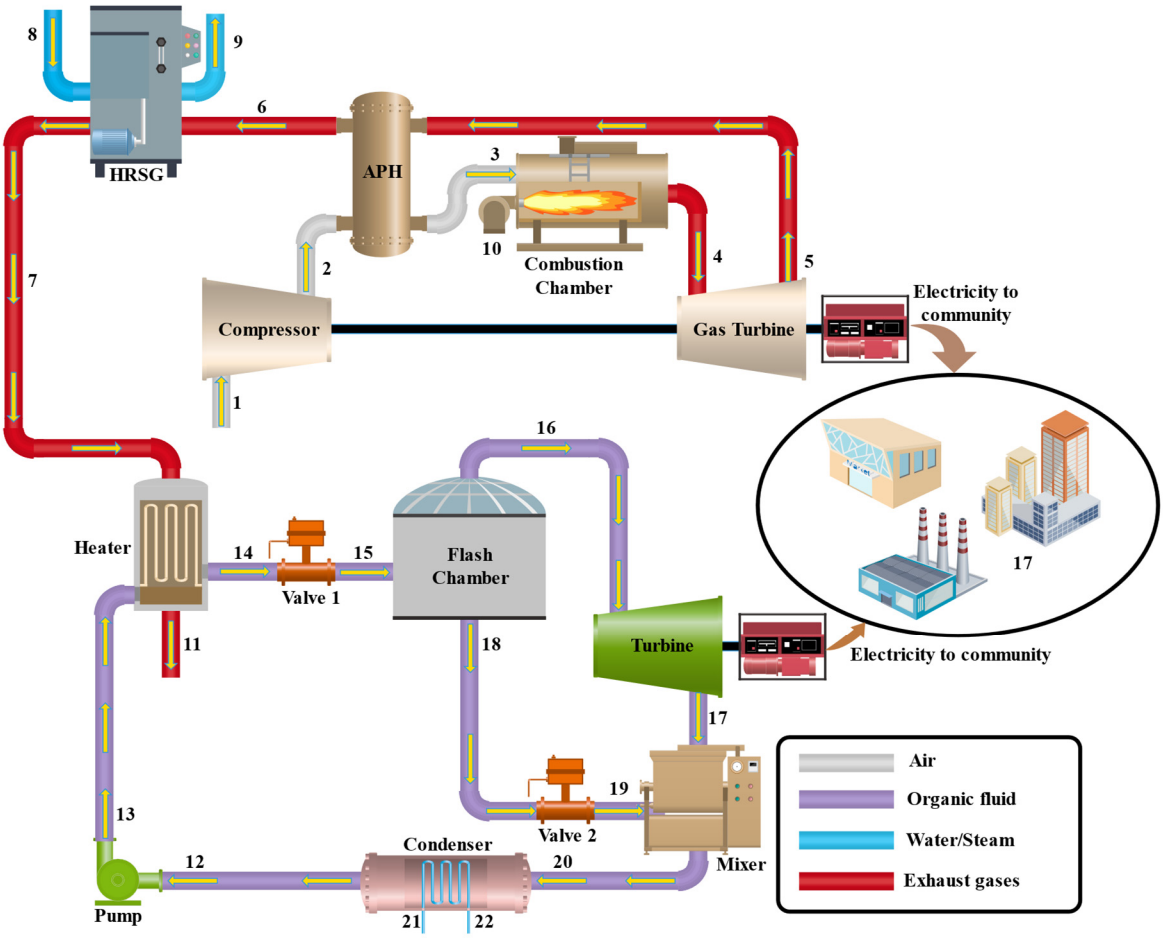

Figure 1. Thermodynamic configuration of the proposed combined GT-OFC plant.

In Figure 1, the air compressor (AC) compresses ambient air at state 1. The compressed air (state 2) receives energy from exhaust gases leaving the air preheater (APH), and the heated air at state 3 flows into the combustion chamber (CC). The combustion chamber receives an injection of fuel at state 10. In the gas turbine (GT), the exhaust gases at state 4 were used to generate electricity. At state 5, the gases enter the APH and exchange heat with air. Following that, the exhaust gases (state 6) from the APH flow to the heat recovery steam generator (HRSG) and generate high-temperature vapor. The cooled gases at state 7 transfer heat to the bottoming cycle (OFC) through a heater. The OFC consists of a pump, valves 1 and 2, a flash separator, a turbine, a mixer, and a condenser. The organic working fluid (state 12) is pumped to the operating pressure of the heater in the saturated liquid phase. The fluid then enters the heater at state 13 and is heated by the exhaust gases. Across valve 1, the high-temperature flow (state 14) then expands. The flash separator separates the two-phase working fluid (state 15) into a saturated liquid (state 18) and a saturated vapor (state 16). The saturated vapor (state 16) generates electricity by expanding in the turbine and subsequently flows into the mixer (state 17). In valve

2, the saturated liquid (state 18) expands before entering the mixer (state 19). After that, the expanded stream from the turbine (state 17) and the expanded stream leaving valve 2 (state 19) are mixed. Finally, in the condenser, cooling water was employed to cool the mixture (state 20).

The working fluid selected for the OFC is a significant factor as it has a direct impact on the system performances from environmental, economic, and thermodynamic perspectives. Some significant criteria should be observed when choosing a suitable working fluid, including the following:

- A dry working fluid whose slope of its vapor saturation curve is positive is preferred [58].
- A working fluid is recommended with low operating pressure and high operating temperature, respectively [59,60]. At high pressures, the compressive stress increases and expensive procedures are required, thus employing a fluid with a high critical pressure is not economically viable.
- Aside from technical criteria, safety issues should be noted. Therefore, it is important to select working fluids with non-flammable, non-toxic, non-explosive, and non-radioactive characteristics [61].
- Ecological and environmental issues need to be considered. The superior organic working fluid is a fluid with low values of ozone depletion potential (ODP) and global warming potential (GWP) [55].

According to the parameters noted above, six organic working fluids are considered here for the OFC. Table 1 presents these working fluids with their thermophysical and environmental characteristics.

Table 1. Critical pressures and temperatures of six organic working fluids utilized in the present GT-OFC plant.

Working Fluid	Thermophysical Characteristics		Environmental Characteristics	
	Critical Temperature (K)	Critical Pressure (kPa)	ODP	GWP (100 Years) (Relative to CO_2)
R245fa	427.2 [62]	3640 [62]	0 [58]	950 [58]
n-Pentane	469.7 [62]	3370 [62]	0 [63]	0 [63]
n-Hexane	507.82 [62]	3034 [62]	0 [63]	0 [63]
n-Heptane	540.13 [62]	2736 [62]	0 [64]	3 [64]
n-Octane	569.32 [62]	2497 [62]	0 [65]	Low [65]
n-Nonane	594.55 [62]	2281 [62]	0	Low

The following assumptions were made for modeling the system:

I. The proposed plant is in steady-state operation.
II. Potential and kinetic energy rates of the components are constant [23].
III. Pressure losses in the air preheater are 5% on the air side and 3% on the gas side. Moreover, pressure losses on the gas side of the HRSG and in the combustion chamber are 5% [66].
IV. Both combustion gases and air exhibit ideal gas behavior [66].
V. Ambient air has the following molar composition (%): 77.48 N_2, 20.59 O_2, 1.90 H_2O (g), 0.03 CO_2 [66].
VI. Pure methane is utilized as the fuel and taken to behave as an ideal gas [66].
VII. The combustion chamber efficiency is considered to be 98%, while other components operate adiabatically [66].
VIII. Pressure and thermal energy losses are ignored in all components of the OFC.
IX. Enthalpies at the inlet and exit of valves are assumed equal [49].
X. At the pump and valve 1 inlets, the organic working fluid's phase is saturated liquid [51].

When dealing with data and making assumptions, there are several potential challenges and uncertainties that can arise. These challenges can impact the accuracy and reliability of analyses, predictions, and decision-making processes. Here are some key areas of concern:

1. Data quality: The quality of data can vary significantly, and there may be issues such as missing values, outliers, measurement errors, or inconsistencies. Incomplete or inaccurate data can lead to biased or flawed results.
2. Uncertain assumptions: Analytical models and algorithms often rely on assumptions about the data and underlying relationships. However, these assumptions may not always hold true in real-world scenarios. Inaccurate or unrealistic assumptions can undermine the validity of results.
3. Future uncertainty: Predictive models are often based on historical data and assume that future patterns will resemble the past. However, disruptive events, changing trends, or unforeseen circumstances can render these models ineffective or inaccurate.

Data used to simulate and model the combined GT-OFC plant are given in Table 2.

Table 2. Input data employed to simulate the combined GT-OFC plant.

System	Parameter	Value	Reference
Gas turbine (GT) cycle	Air compressor pressure ratio, r_{AC}	7–20	[66]
	Net power generated in the GT system, $\dot{W}_{net,GT}$ (MW)	30	[66]
	Gas turbine isentropic efficiency, η_{GT} (%)	81–91	[31]
	Air compressor isentropic efficiency, η_{AC} (%)	78–89	[31]
	Preheated air temperature, T_3 (K)	820–940	[31]
	Combustion chamber outlet temperature, T_4 (K)	1520	[31]
	Pinch point temperature difference in the HRSG, $\Delta T_{pp,HRSG}$ (K)	8–30	[31]
	HRSG inlet temperature, T_8 (K)	298.15	[66]
	Pressure of inlet water to the HRSG, P_8 (bar)	35	[31]
	Inlet temperature of the fuel flowing into the combustion chamber, T_{10} (K)	298.15	[66]
	Pressure of inlet fuel to the combustion chamber, P_{10}	12	[31]
	Methane lower heating value, LHV (kJ/kmol)	802,661	[66]
	Unit cost of exergy of methane, c_{10} ($/GJ)	10	[67]
Organic flash cycle (OFC)	Inlet temperature of the flash separator, T_{15} (K)	333.2–371.2	[54]
	Turbine isentropic efficiency, η_T (%)	0.8	[54]
	Pump isentropic efficiency, η_P (%)	0.8	[54]
	Pinch point temperature difference in the condenser, $\Delta T_{pp,Cond}$ (K)	10	[54]
	Terminal temperature difference in the heater, ΔT_{Heater} (K)	8–16	[54]
Economic input data	Interest rate, i_r (%)	12	[55]
	Operation years, N	20	[55]
	Annual plant operation hours, t	8000	[55]
	Maintenance factor, γ	0.06	[55]
Ambient conditions	Ambient temperature, T_0 (K)	298.2	
	Ambient Pressure, P_0 (bar)	1	

3. Modeling and Analysis

The EES software version 9.478 is employed to simulate the hybrid GT-OFC plant, utilizing equations that govern the conservation of mass, energy, and exergy balances as the fundamental basis for modeling process. Furthermore, the cost balance is applied to each component within the combined system and an environmental assessment is included to evaluate the ecological impact of the plant, thereby ensuring a comprehensive investigation. All system components are considered as control volumes during the analysis.

3.1. Mass and Energy Conservations

Given the assumptions applied, mass and energy conservation relations can be expressed as [68]:

$$\sum \dot{m}_{in} = \sum \dot{m}_{out} \quad (1)$$

$$\sum \dot{m}_{in} h_{in} - \sum \dot{m}_{out} h_{out} + \sum \dot{Q} - \sum \dot{W} \tag{2}$$

where $\dot{m}$, $\dot{Q}$, $\dot{W}$, and h denote mass flow rate, heat transfer rate, the mechanical power, and the specific enthalpy, respectively. Moreover, subscripts in and out represent inlet and outlet flows into the control volume. Equations relevant to the conservation of mass and energy for each component of the GT-OFC system are shown in Table 3.

Table 3. Mass and energy conservation relations and other expressions for each component of the GT-OFC plant.

Component	Conservation of Mass	Conservation of Energy and Other Expressions
Air compressor	$\dot{m}_1 = \dot{m}_2$	$\dot{m}_1 h_1 + \dot{W}_{AC} = \dot{m}_2 h_2$ $\eta_{AC} = \frac{h_{2s} - h_1}{h_2 - h_1}$
Air preheater	$\dot{m}_2 = \dot{m}_3$ and $\dot{m}_5 = \dot{m}_6$	$\dot{m}_3(h_3 - h_2) = \dot{m}_5(h_5 - h_6)$
Combustion chamber	$\dot{m}_3 = \dot{m}_4$	$\dot{m}_3 h_3 + 0.98\dot{m}_f LHV = \dot{m}_4 h_4$
Gas turbine	$\dot{m}_4 = \dot{m}_5$	$\dot{m}_4 h_4 = \dot{m}_5 h_5 + \dot{W}_{GT}$ $\eta_{GT} = \frac{(h_4 - h_5)}{(h_4 - h_{5s})}$
HRSG	$\dot{m}_6 = \dot{m}_7$ and $\dot{m}_8 = \dot{m}_9$	$\dot{m}_6(h_6 - h_7) = \dot{m}_9(h_9 - h_8)$
Heater	$\dot{m}_7 = \dot{m}_{11}$ and $\dot{m}_{13} = \dot{m}_{14}$	$\dot{m}_7(h_7 - h_{11}) = \dot{m}_{13}(h_{14} - h_{13})$
Pump	$\dot{m}_{12} = \dot{m}_{13}$	$\dot{m}_{12} h_{12} + \dot{W}_P = \dot{m}_{13} h_{13}$ $\eta_P = \frac{(h_{13s} - h_{12})}{(h_{13} - h_{12})}$
Valve 1	$\dot{m}_{14} = \dot{m}_{15}$	$\dot{m}_{14} h_{14} = \dot{m}_{15} h_{15}$
Flash separator	$\dot{m}_{15} = \dot{m}_{16} + \dot{m}_{18}$	$\dot{m}_{15} h_{15} = \dot{m}_{16} h_{16} + \dot{m}_{18} h_{18}$
Turbine	$\dot{m}_{16} = \dot{m}_{17}$	$\dot{m}_{16} h_{16} = \dot{m}_{17} h_{17} + \dot{W}_T$ $\eta_T = \frac{(h_{16} - h_{17})}{(h_{16} - h_{17s})}$
Valve 2	$\dot{m}_{18} = \dot{m}_{19}$	$\dot{m}_{18} h_{18} = \dot{m}_{19} h_{19}$
Mixer	$\dot{m}_{20} = \dot{m}_{17} + \dot{m}_{19}$	$\dot{m}_{20} h_{20} = \dot{m}_{17} h_{17} + \dot{m}_{19} h_{19}$
Condenser	$\dot{m}_{12} = \dot{m}_{20}$ and $\dot{m}_{21} = \dot{m}_{22}$	$\dot{m}_{20}(h_{20} - h_{12}) = \dot{m}_{21}(h_{22} - h_{21})$

An important objective function is the system energy efficiency, which can be computed as follows:

$$\eta_{th} = \frac{\dot{W}_{net,tot} + (\dot{E}_9 - \dot{E}_8)}{\dot{m}_f LHV} \tag{3}$$

3.2. Exergy Analysis

Exergy analysis is another variable considered to investigate the system performance. It plays a noteworthy role in the system improvement by determining the quantities of exergy destruction rates and other important parameters. Exergy analysis provides researchers with information about which components should be enhanced to reduce exergy destruction. The exergy rate balance for a component at steady-state operation is expressed as:

$$\dot{E}_Q + \sum \dot{E}_{in} - \dot{W} - \sum \dot{E}_{out} = \dot{E}_D \tag{4}$$

where $\dot{E}_Q$, $\dot{E}_{in}$, $\dot{E}_{out}$, and $\dot{E}_D$ are the exergy rates attributable to heat transfer, inlet mass flow to the control volume, outlet mass flow from the control volume, and destruction (irreversibility), respectively.

The combination of chemical and thermomechanical exergies determines the total exergy of a flow stream. The greatest theoretical work that is achievable as a system reaches the restricted dead state from its initial condition is known as thermomechanical exergy.

Thermomechanical exergy comprises kinetic, potential, and physical exergies, and the first two initial terms are often neglected. Therefore, the thermomechanical exergy comprises the physical exergy, which can be calculated as follows [54]:

$$\dot{E}_{ph} = \dot{m}[(h - h_0) - T_0(s - s_0)] \tag{5}$$

where s is the specific entropy.

The molar chemical exergy can be expressed as [31]:

$$\overline{e}_{ch} = \sum_{k=0}^{n} x_k \overline{e}_k^{ch} + \overline{R}T_0 \sum_{k=0}^{n} x_k \ln x_k \tag{6}$$

where x_k is the gas mole fraction. Table 4 summarizes the exergy rate balances of each component of the GT-OFC cycle.

Table 4. Exergy rate balance for each component of the GT-OFC plant.

Component	Exergy Rate Balance
Air compressor	$\dot{E}_{D,AC} = \dot{E}_1 + \dot{W}_{AC} - \dot{E}_2$
Air preheater	$\dot{E}_{D,APH} = \dot{E}_2 + \dot{E}_5 - \dot{E}_3 - \dot{E}_6$
Combustion chamber	$\dot{E}_{D,CC} = \dot{E}_3 + \dot{E}_{10} - \dot{E}_4$
Gas turbine	$\dot{E}_{D,GT} = \dot{E}_4 - \dot{E}_5 - \dot{W}_{GT}$
HRSG	$\dot{E}_{D,HRSG} = \dot{E}_6 + \dot{E}_8 - \dot{E}_7 - \dot{E}_9$
Heater	$\dot{E}_{D,Heater} = \dot{E}_7 + \dot{E}_{13} - \dot{E}_{11} - \dot{E}_{14}$
Pump	$\dot{E}_{D,P} = \dot{W}_P + \dot{E}_{12} - \dot{E}_{13}$
Valve 1	$\dot{E}_{D,V1} = \dot{E}_{14} - \dot{E}_{15}$
Flash separator	$\dot{E}_{D,FS} = \dot{E}_{15} - \dot{E}_{16} - \dot{E}_{18}$
Turbine	$\dot{E}_{D,T} = \dot{E}_{16} - \dot{E}_{17} - \dot{W}_T$
Valve 2	$\dot{E}_{D,V2} = \dot{E}_{18} - \dot{E}_{19}$
Mixer	$\dot{E}_{D,Mixer} = \dot{E}_{17} + \dot{E}_{19} - \dot{E}_{20}$
Condenser	$\dot{E}_{D,Cond} = \dot{E}_{20} + \dot{E}_{21} - \dot{E}_{12} - \dot{E}_{22}$

In addition to exergy destruction, the exergy loss of the condenser is calculated as follows:

$$\dot{E}_{L,Cond} = \dot{E}_{22} - \dot{E}_{21} \tag{7}$$

It is insightful to determine the system exergy efficiency. For the suggested plant, the efficiency can be represented as follows [31]:

$$\eta_{ex} = \frac{\dot{W}_{net,tot} + (\dot{E}_9 - \dot{E}_8)}{(\dot{E}_1 + \dot{E}_{10})} \tag{8}$$

3.3. Environmental Analysis

Since the utilization of fossil fuels for power generation results in pollutant emissions such as NOx, carbon dioxide (CO_2), and carbon monoxide (CO), evaluating a system solely from thermodynamics viewpoint is not comprehensive and is potentially ineffective from a holistic perspective. As a result, environmental factors need to be considered. The generation of NOx and CO is affected by the combustion temperature [69]. It is possible to calculate the adiabatic flame temperature based on the formula provided in [41]. The amount of NOx and CO produced can be determined as follows [41]:

$$m_{CO} = \frac{0.179 \times 10^9 \exp(\frac{7800}{T_{pz}})}{P_3^2 \tau [\frac{\Delta P_{cc}}{P_3}]^{0.5}} \tag{9}$$

$$m_{NOx} = 0.459 \times 10^{-8} P_3^{0.25} \tau \exp(0.01 T_{pz}) \tag{10}$$

where m_{CO} and m_{NOx} are the masses of CO and NOx produced in units of $g_{pollutant}/kg_{fuel}$, T_{pz} is the adiabatic flame temperature, ΔP_{cc} denotes the pressure reduction in the combustion chamber, and τ is the residence time, which was taken here to be 0.002 s [69]. Furthermore, the amount of CO_2 emission can be evaluated with a carbon balance in the combustion chamber [70].

The levelized total emission (LTE) is utilized to determine the ratio of the total mass flow rate of greenhouse gases during the lifetime of the plant to the total net produced power.

$$LTE(\text{kg/kW}) = \frac{(\dot{m}_{CO} + \dot{m}_{CO2} + \dot{m}_{NOx})(3600 \times t \times N)}{\dot{W}_{net,tot}} \tag{11}$$

Here, N and t are the operation years and annual plant operation hours, respectively.

3.4. Exergo-Economic Analysis

To investigate the system economically, exergo-economic analysis is applied. This method combines economics and exergy and delivers useful information about the system from economics standpoint. These results are often required for designing the system. Many approaches to exergo-economic analysis have been proposed, including the exergy cost theory [71], average cost method [72], and specific exergy costing (SPECO) [73–76]. In this work, the SPECO approach is applied. It has three stages: (a) analyzing energy and exergy attributes for each state; (b) specifying products and fuels for each component of the system; and (c) creating cost balances and ancillary equations for each component.

The cost rate balance for a component under steady-state operation can be expressed as [66]:

$$\sum \dot{C}_{out,k} + \dot{C}_{w,k} = \dot{C}_{in,k} + \dot{C}_{q,k} + \dot{Z}_k \tag{12}$$

$$\dot{C} = c\dot{E} \tag{13}$$

where $\dot{C}_{w,k}$, $\dot{C}_{q,k}$, and $\dot{Z}_k$ are the rates of costs associated with produced work, heat transfer, and the capital cost of component k, respectively. Table 5 lists the ancillary equations and cost rate balance for each system component.

Table 5. Cost rate balance and ancillary equations for each component of the GT-OFC plant.

Component	Cost Rate Balance Equation	Ancillary Equation
Air compressor	$\dot{C}_1 + \dot{C}_{w,AC} + \dot{Z}_{AC} = \dot{C}_2$	$\dot{C}_1 = 0$
Air preheater	$\dot{C}_2 + \dot{C}_5 + \dot{Z}_{APH} = \dot{C}_3 + \dot{C}_6$	$c_6 = c_5$
Combustion chamber	$\dot{C}_3 + \dot{C}_{10} + \dot{Z}_{cc} = \dot{C}_4$	–
Gas turbine	$\dot{C}_4 + \dot{Z}_{GT} = \dot{C}_5 + \dot{C}_{w,GT}$	$c_5 = c_4$ and $\frac{\dot{C}_{w,AC}}{\dot{W}_{AC}} = \frac{\dot{C}_{w,GT}}{\dot{W}_{Gt}}$
HRSG	$\dot{C}_6 + \dot{C}_8 + \dot{Z}_{HRSG} = \dot{C}_7 + \dot{C}_9$	$c_7 = c_6$
Heater	$\dot{C}_{13} + \dot{C}_7 + \dot{Z}_{Heater} = \dot{C}_{14} + \dot{C}_{11}$	$c_{11} = c_7$
Pump	$\dot{C}_{12} + \dot{C}_{w,p} + \dot{Z}_P = \dot{C}_{13}$	$\frac{\dot{C}_{w,P}}{\dot{W}_P} = \frac{\dot{C}_{w,T}}{\dot{W}_T}$
Valve 1	$\dot{C}_{14} + \dot{Z}_{V1} = \dot{C}_{15}$	–
Flash separator	$\dot{C}_{15} + \dot{Z}_{FS} = \dot{C}_{16} + \dot{C}_{18}$	$\frac{(\dot{C}_{16} - \dot{C}_{15})}{(\dot{E}_{16} - \dot{E}_{15})} = \frac{(\dot{C}_{18} - \dot{C}_{15})}{(\dot{E}_{18} - \dot{E}_{15})}$
Turbine	$\dot{C}_{16} + \dot{Z}_T = \dot{C}_{17} + \dot{C}_{w,T}$	$c_{16} = c_{17}$
Valve 2	$\dot{C}_{18} + \dot{Z}_{V2} = \dot{C}_{19}$	–
Mixer	$\dot{C}_{17} + \dot{C}_{19} + \dot{Z}_{Mixer} = \dot{C}_{20}$	–
Condenser	$\dot{C}_{20} + \dot{C}_{21} + \dot{Z}_{Cond} = \dot{C}_{12} + \dot{C}_{22}$	$c_{12} = c_{20}$ and $\dot{C}_{21} = 0$

The sum of the annualized capital cost investment and the operating and maintenance costs of component k constitutes the capital cost rate of the system, which is calculated as [66]:

$$\dot{Z}_k = \dot{Z}_k^{CI} + \dot{Z}_k^{OM} \tag{14}$$

$$\dot{Z}_k = (\frac{CRF + \gamma}{t})Z_k \tag{15}$$

Here, γ, Z_k, and CRF are the maintenance factor, the capital cost of the component k, and the capital recovery factor. CRF can be written as follows [66]:

$$CRF = \frac{i_r(1+i_r)^N}{(1+i_r)^N - 1} \tag{16}$$

where i_r is the interest rate. Table 2 provides the values of t, N, γ, and i_r. For the economic investigation of the proposed system, the computation of the capital cost of the kth component is necessary. Table 6 provides the function associated with the capital cost for each system component.

Table 6. Cost functions and $CEPCI_0$ for each GT-OFC plant component.

Component	Cost Function	Original Year	$CEPCI_0$	Reference
Air compressor	$Z_{AC} = \frac{71.1\dot{m}_1}{0.9-\eta_{AC}} \frac{P_2}{P_1} \ln \frac{P_2}{P_1}$	1995	381.1	[66]
Air preheater	$Z_{APH} = 4122(\frac{\dot{m}_4(h_5-h_6)}{U\Delta T_{LMTD,APH}}), U = 18\frac{W}{m^2K}$	1995	381.1	[66]
Combustion chamber	$Z_{cc} = (\frac{46.08\dot{m}_3}{0.995-(\frac{P_4}{P_3})})(1+\exp(0.018T_4 - 26.4)$	1995	381.1	[66]
Gas turbine	$Z_{GT} = (\frac{479.34\dot{m}_4}{0.92-\eta_{GT}}) \ln(\frac{P_4}{P_5})[1+\exp(0.036T_4 - 54.4]$	1995	381.1	[66]
HRSG	$Z_{HRSG} = 6570[(\frac{\dot{Q}_{ec}}{\Delta T_{LMTD,ec}})^{0.8} + (\frac{\dot{Q}_{ev}}{\Delta T_{LMTD,ev}})^{0.8}] + 21276\dot{m}_8 + 1184.4\dot{m}_4{}^{1.2}$	1995	381.1	[66]
Heater	$Z_{Heater} = 2681A_{Heater}^{0.59}, U_{Heater} = 1600(\frac{W}{m^2K})$	1986	318.4	[55]
Pump	$Z_P = 1120\dot{W}_P^{0.8}$	2005	468.2	[55]
Turbine	$Z_T = 4405\dot{W}_T^{0.7}$	2005	468.2	[55]
Condenser	$Z_{Cond} = 2143A_{Cond}^{0.514}, U_{Cond} = 2000(\frac{W}{m^2K})$	1986	318.4	[55]

The cost functions of the heat exchangers depend on the heat transfer area, which can be expressed as:

$$A_k = \frac{\dot{Q}_k}{U_k \Delta T_{LMTD,k}} \tag{17}$$

Here, $\Delta T_{LMTD,k}$, $\dot{Q}_k$, and U_k are the logarithmic mean temperature difference, the heat transfer rate, and the total heat transfer coefficient, respectively. Here, costs for the valves, mixer, and flash separator are neglected [55,77,78]. The source costs in Table 6 are translated into 2021 costs utilizing the chemical engineering plant cost index (CEPCI), as follows:

$$Z_{2021} = \frac{Z_{original} CEPCI_{2021}}{CEPCI_0} \tag{18}$$

where the $CEPCI_{2021}$ value stands at 766.9 [79].

The last performance parameter, which is the rate of total cost of the overall system, can be represented as:

$$\dot{C}_{tot} = \sum \dot{Z}_k + \sum \dot{C}_{D,k} + \dot{C}_{env} + \dot{C}_{fuel} \tag{19}$$

where $\dot{C}_{fuel}$, $\dot{C}_{env}$, and $\sum \dot{C}_{D,k}$ denote the cost rates related to fuel, the environment, and destruction, respectively. These can be calculated as follows [80]:

$$\dot{C}_{fuel} = c_{10}\dot{n}_{fuel}LHV \tag{20}$$

where LHV and $\dot{n}_{fuel}$ are the lower heating value of methane and the molar flow rate. Also,

$$\dot{C}_{env} = c_{NOx}\dot{m}_{NOx} + c_{CO}\dot{m}_{CO} + c_{CO2}\dot{m}_{CO2} \tag{21}$$

$$\dot{C}_{D,k} = c_{F,k}\dot{E}_{D,k} \tag{22}$$

where c_{NOx}, c_{CO}, and c_{CO2} are specific costs associated with NOx, CO, and CO_2 emissions. These values are taken here to be 6.853 \$/kg, 0.2086 \$/kg [31], and 0.024 \$/kg [81], respectively. $c_{F,k}$ represents the average cost per unit exergy of fuel for a general component.

Useful information can be provided by the exergo-economic factor, which is defined as:

$$f_k = \frac{\dot{Z}_k}{\dot{Z}_k + \dot{C}_{D,k} + \dot{C}_{L,k}} \tag{23}$$

3.5. Validation

In Table 7, the current study's simulation results using the EES software are compared to the findings from previous works. In this comparison, the results published in [54,66] are applied to validate the GT system and the OFC, respectively. According to Table 7, the maximum inaccuracy is 1.95%, suggesting that the simulation findings are in good agreement with the reference data.

Table 7. Validation of results for the GT and the OFC sub-systems.

System	Parameter	Present Work	Reference Value	Error (%)
GT cycle [66]	λ	0.0323	0.0321	0.62
	T_1 (K)	298.15	298.15	0.00
	T_2 (K)	610.85	603.738	1.18
	T_3 (K)	850	850	0.00
	T_4 (K)	1520	1520	0.00
	T_5 (K)	1012.4	1006.1	0.63
	T_6 (K)	795	779.78	1.95
	T_{10} (K)	298.15	298.15	0.00
	P_1 (bar)	1.013	1.013	0.00
	P_2 (bar)	10.13	10.13	0.00
	P_3 (bar)	9.624	9.623	0.01
	P_4 (bar)	9.142	9.142	0.00
	P_5 (bar)	1.1	1.09	0.92
	P_6 (bar)	1.063	1.067	0.38
	P_{10} (bar)	12	12	0
	$\dot{W}_{GT}$ (MW)	30	30	0

Table 7. *Cont.*

System	Parameter	Present Work	Reference Value	Error (%)
OFC [54]	T_{12} (°C)	40	40	0.00
	T_{13} (°C)	40.55	40.70	0.37
	T_{15} (°C)	80	80	0.00
	T_{16} (°C)	80	80	0.00
	T_{17} (°C)	51.04	51.18	0.27
	T_{18} (°C)	80	80	0.00
	T_{19} (°C)	40	40	0.00
	T_{20} (°C)	40	40	0.00

3.6. Multi-Objective Optimization

MOO seeks to optimize multiple performance parameters simultaneously. Genetic algorithms are optimization techniques inspired by the process of natural selection and genetics. In the context of energy systems, genetic algorithms can be used to optimize various aspects such as energy generation, distribution, and consumption. It involves creating a population of potential solutions represented as chromosomes and applying genetic operators such as selection, crossover, and mutation to evolve and improve these solutions over cogeneration and multigeneration systems. The fitness of each solution is evaluated based on predefined criteria, such as exergy efficiency, cost-effectiveness, and environmental impact. By iteratively applying these genetic operations, the algorithm converges towards an optimal solution that meets the desired objectives for system optimization. Using EES software, environmental, exergo-economic, and thermodynamic investigations of the proposed cogeneration system are carried out. To perform MOO utilizing genetic algorithm, EES software and MATLAB software version R2015a are connected to each other.

The primary objectives of the MOO in the current combined plant involve the LTE, total cost rate, and exergy efficiency. The MOO approach presented in this research seeks to minimize the system total cost rate and LTE while maximizing the exergy efficiency of the overall system. Table 8 provides the specified lower and upper bounds for the decision variables in the proposed optimization.

Table 8. Lower and upper values of the decision variables for the proposed optimizations.

Decision Variable	Lower Bound	Upper Bound
Air compressor pressure ratio	7	20
Preheated air temperature (K)	820	940
Pinch point temperature difference in the HRSG (K)	8	30
Terminal temperature difference in the heater (K)	8	16

The MOO based on the genetic algorithm is supported by Table 9, which outlines the primary input variables.

Table 9. Main input variables for the genetic algorithm-based MOO [82,83].

Variable	Value
Population size	500
Maximum number of generations	600
Probability of crossover	85%
Probability of mutation	1%
Tournament size	2

4. Results and Discussion

Table 10 presents the thermodynamic properties and the energy cost data for the combined GT-OFC system using R245fa as the working fluid in the OFC, based on the initial

design conditions. At state 7, the combustion gases enter the heater and heat stream 13 in the low-temperature cycle at the temperature of 382.1 K. The outlet flow from the heater exits at state 8 with the temperature of 323.7 K. Additionally, water enters the HRSG at the pressure of 35 bar and the temperature of 298 K, and it is transformed into saturated vapor at 515.8 K. The mass flow rate of water used to produce saturated vapor is 15.9 kg/s.

Table 10. Thermodynamic characteristics and exergy flow cost data for the GT-OFC plant [a].

Stream	Fluid	T (K)	P (bar)	$\dot{m}$ (kg/s)	$\dot{E}_{ph}$ (MW)	$\dot{E}_{ch}$ (MW)	$\dot{E}$ (MW)	$\dot{C}$ ($/h)	c ($/GJ)
1	Air	298.2	1.013	92.6	0	0	0	0	0
2	Air	610.9	10.13	92.6	27.75	0	27.75	2636	26.38
3	Air	850	9.624	92.6	41.55	0	41.55	3912	26.15
4	Comb. gases	1520	9.142	94.26	99.63	0.385	100	7629	21.19
5	Comb. gases	1012	1.11	94.26	37.64	0.385	38.02	2900	21.19
6	Comb. gases	795.1	1.077	94.26	21.48	0.385	21.86	1667	21.19
7	Comb. gases	382.1	1.044	94.26	1.219	0.385	1.604	122.3	21.19
8	Water	298.2	35	15.9	0.054	0.040	0.094	0	0
9	Water	515.8	35	15.9	15.6	0.040	15.64	1643	29.18
10	Methane	298.2	12	1.655	0.632	85.02	85.65	3700	12
11	Comb. gases	323.7	1.013	94.26	0.101	0.385	0.486	37.06	21.19
12	R245fa	313.2	2.496	68.19	0.488	_	0.488	109.5	62.33
13	R245fa	313.7	12.39	68.19	0.541	_	0.541	127.2	65.34
14	R245fa	372.1	12.39	68.19	1.294	_	1.294	217.5	46.68
15	R245fa	353.2	7.908	68.19	1.229	_	1.229	217.5	49.16
16	R245fa	353.2	7.908	12.91	0.482	_	0.482	85.31	49.16
17	R245fa	324.2	2.496	12.91	0.214	_	0.214	37.88	49.16
18	R245fa	353.2	7.908	55.28	0.747	_	0.747	132.2	49.16
19	R245fa	313.2	2.496	55.28	0.546	_	0.546	132.2	67.22
20	R245fa	313.2	2.496	68.19	0.758	_	0.758	170.1	62.33
21	Water	298.2	1.013	268.4	0	_	0	0	0
22	Water	303.2	1.013	268.4	0.049	_	0.049	62.58	354.7

[a] $r_{AC} = 10$, $\eta_{GT} = \eta_{AC} = 86$ (%), $T_3 = 850$ (K), $T_4 = 1520$ (K), $\Delta T_{pp,HRSG} = 15$ (K), $T_{15} = 353.15$ (K), $\Delta T_{pp,Cond} = 10$ (K), $\Delta T_{Heater} = 10$ (K).

4.1. Results of Energy, Exergy, Exergo-Economic, and Environmental Assessments

The findings of the combined GT-OFC system's environmental, exergo-economic, exergy, and energy assessments are shown in Table 11 using base design circumstances with R245fa as the working fluid. The cycle net output power was observed to be 30 MW. By employing the bottoming cycle of OFC, the net output power of the system increased by 153 kW. In addition, utilizing the GT system's waste heat in the heater leads to an increase in the exergy efficiency of the system by 0.32%.

Table 11. Findings of environmental, economic, exergy, and energy assessments of the GT-OFC plant using R245fa under base design conditions.

Parameter	Value
$\dot{W}_{net,tot}$ (kW)	30,153
$\dot{W}_{GT}$ (MW)	30
$\dot{W}_{OFC}$ (KW)	153
$\eta_{I,GT}$ (%)	55.02
$\eta_{I,GT-OFC}$ (%)	55.20
$\eta_{II,GT}$ (%)	53.18
$\eta_{II,GT-OFC}$ (%)	53.35
$\dot{C}_{tot}$ ($/h)	7422
LTE (kg/kW)	89,383

The findings indicate that incorporating the bottoming cycle enhances the overall performance of the system in terms of exergy and energy efficiencies. When evaluating the system from economic perspective, the total cost rate is studied and determined to be 7332 $/h under the base design conditions. The majority of this cost is attributed to the fuel expenses. By reducing fuel consumption, the associated cost is also reduced. Consequently, employing methods that minimize fuel utilization has an impact on the total cost rate of the system. The long-term exergy (LTE) value, which is calculated as 89,363 kg/kW over a 20 year period per unit of net output power, demonstrates that increasing the system's net output power results in a decrease in the LTE value, as indicated by Equation (11).

Table 12 shows the system performance results from economic and exergy viewpoints. Among the combined GT-OFC system components, the highest exergy destruction rate is attributable to the combustion chamber, at 27.19 MW. Overall, 69% of the overall destruction of exergy of the entire system is due to the destruction of exergy in the combustion chamber. In addition, due to the large destruction of exergy in the chamber, this component has the highest cost rate of 1627 $/h. The highest exergo-economic factor (f_k) is attributable to the gas turbine (GT), at 53.42%. This value indicates that the cost of the operation and maintenance and capital investment play important roles. Based on Equation (23), as indicated earlier, due to the large cost of the destruction of exergy in the combustion chamber, its exergo-economic factor is low. This shows that the greatest part of the cost rate of the chamber is caused by the cost of exergy destruction. Moreover, the heater and the condenser have poor exergo-economic factors, mainly because of the great costs of exergy destruction in these components. The rates of destroyed exergy and exergo-economic factor of the integrated GT-OFC system are 39.42 MW and 16.45%, respectively.

Table 12. Findings of the exergo-economic and exergy assessments of the integrated GT-OFC plant under base design conditions for all components.

Component	$\dot{E}_{F,k}$(MW)	$\dot{E}_{P,k}$(MW)	$\dot{E}_{D,k}$(MW)	$\dot{E}_{L,k}$(MW)	$\dot{C}_{D,k}$($/h)	$\dot{Z}_k$($/h)	$\dot{C}_{L,k}$($/h)	f_k(%)
Air compressor	29.87	27.75	2.117	0	173.7	184.8	0	51.56
Air preheater	65.78	63.41	2.363	0	198.9	43.33	0	17.89
Combustion chamber	127.2	100.0	27.19	0	1627	16.70	0	1.016
Gas turbine	61.99	59.87	2.123	0	161.9	184.1	0	53.42
HRSG	21.96	17.24	4.711	0.486	357.8	98.06	37.06	19.89
Heater	1.118	0.754	0.364	0	81.31	5.047	0	5.844
Pump	0.065	0.053	0.012	0	3.120	1.254	0	28.66
Valve 1	1.294	1.229	0.065	0	10.95	0	0	-
Flash separator	1.229	1.229	0	0	0	0	0	-
Turbine	0.268	0.218	0.050	0	8.910	7.571	0	45.94
Valve 2	0.747	0.546	0.201	0	35.52	0	0	-
Mixer	0.760	0.758	0.002	0	0.535	0	0	-
Condenser	0.758	0.488	0.221	0.049	49.55	2.036	11	3.254
Overall system	85.65	45.70	39.42	0.535	2709	542.9	48.06	16.45

4.2. Parametric Study

To find out how the decision parameters affect the LTE, exergy efficiency, and total cost rate of the system, a parametric study was applied. The decision parameters are the air compressor pressure ratio, the gas turbine isentropic efficiency, the air compressor isentropic efficiency, the preheated air temperature, the pinch point temperature difference in the HRSG, the flash separator inlet temperature, and the terminal temperature difference of the heater.

In the current system, extensive research in this field has been reviewed, and it has been observed that these seven decision-making parameters are consistently taken into account in analyses. Therefore, these seven parameters have been chosen. Moreover, this choice is based on the decision variables' significant influences on the total cost rate of the system, exergy efficiency, and LTE, and their crucial roles in determining system performance compared with other operational parameters.

Figure 2 depicts the effects of the pressure ratio of the air compressor on the overall system cost rate, LTE, and total exergy efficiency. By boosting r_{AC}, the η_{ex} of the system achieves a local maximum. In contrast, the system $\dot{C}_{tot}$ is minimized with a rise in r_{AC}. LTE also behaves like $\dot{C}_{tot}$ of the system. Owing to the unchanged GT system's net output power, with a rise in r_{AC}, the power used by the air compressor and, consequently, the produced power of the gas turbine increase. This increase results in a local minimum for the mass flow rate of air. In addition, owing to the unchanged combustion chamber inlet and outlet temperatures, the enthalpies of the inlet and outlet streams of the combustion chamber also remain constant. As a consequence, for pressure ratios between 8–13, the rate of fuel consumption in the combustion chamber decreases, while at the pressure ratios larger than 13, the fuel consumption rises, which causes a local minimum for the exergy rate of the required fuel. Because of the variations in the production rate of the combustion gases, there is a local maximum for the heat transfer rate to the bottoming cycle (OFC), which results in local maximum for the OFC's net output power. As mentioned, a rise in the pressure ratio causes a decrease in the input fuel rate, which decreases $\dot{C}_{tot}$ of the system. A further growth in the pressure ratio causes a rise in the OFC working fluid cost rate, which increases the system's $\dot{C}_{tot}$. Referring to the mentioned statements and Figure 2, there is an optimum value for r_{AC}, at which LTE and $\dot{C}_{tot}$ of the system possess the lowest possible values and η_{ex} has the highest value. Bestowing to Figure 2, from environmental, economic, and exergy perspectives, n-nonane has the best performance among considered working fluids of the OFC.

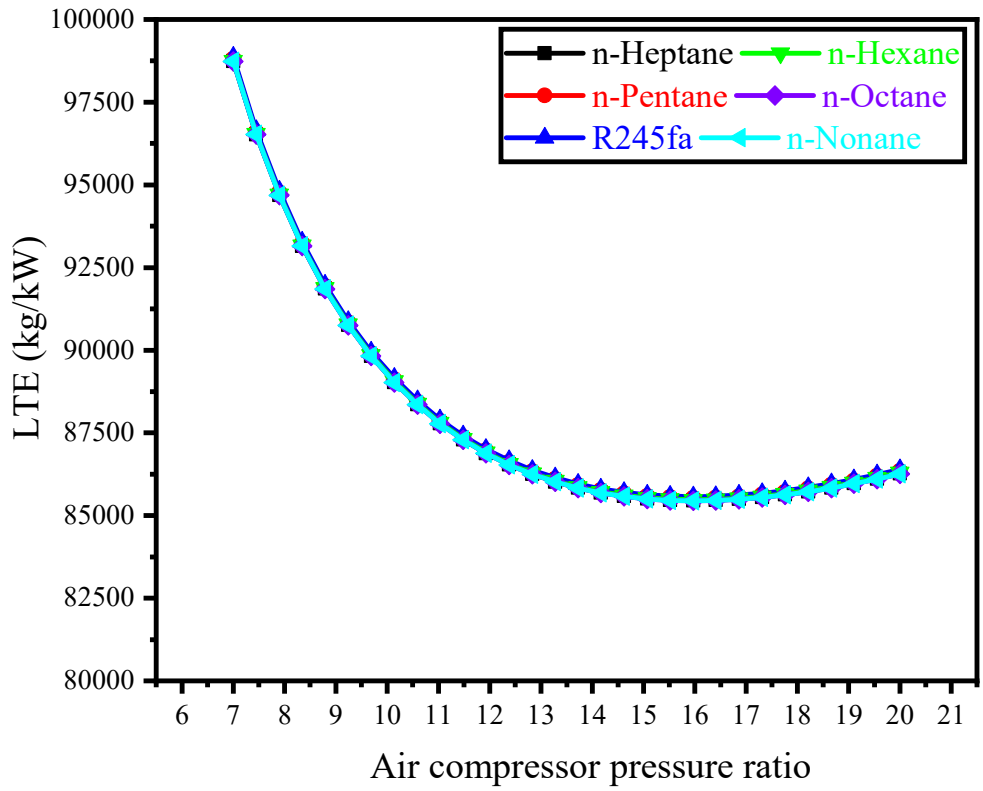

(**a**)

Figure 2. *Cont.*

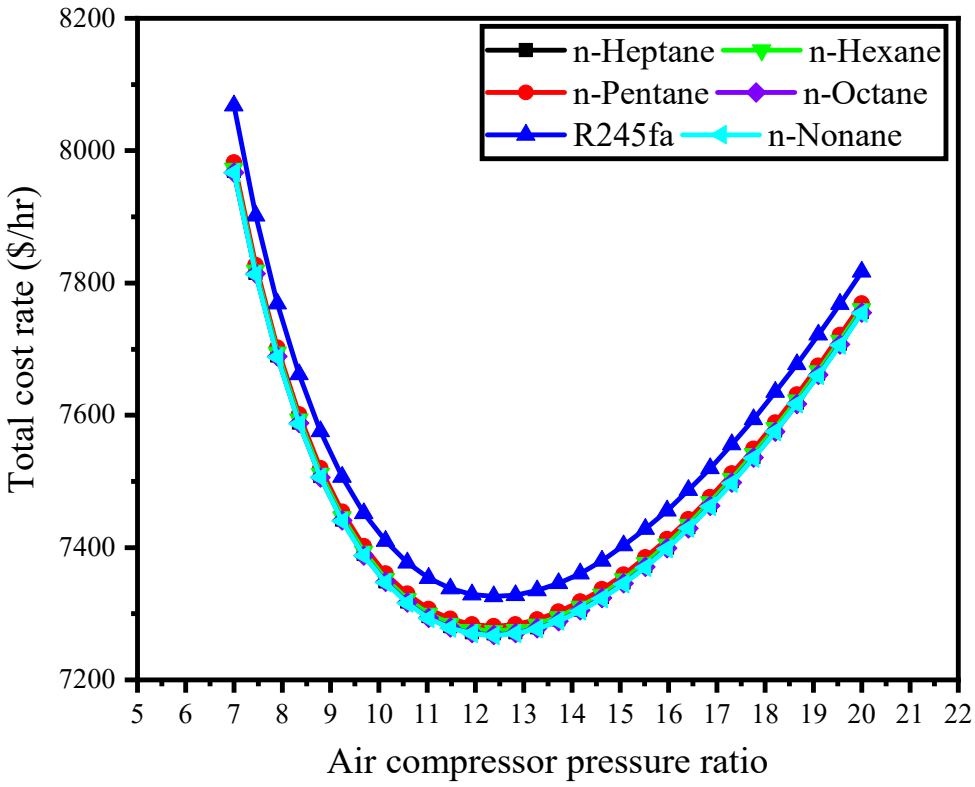

(**b**)

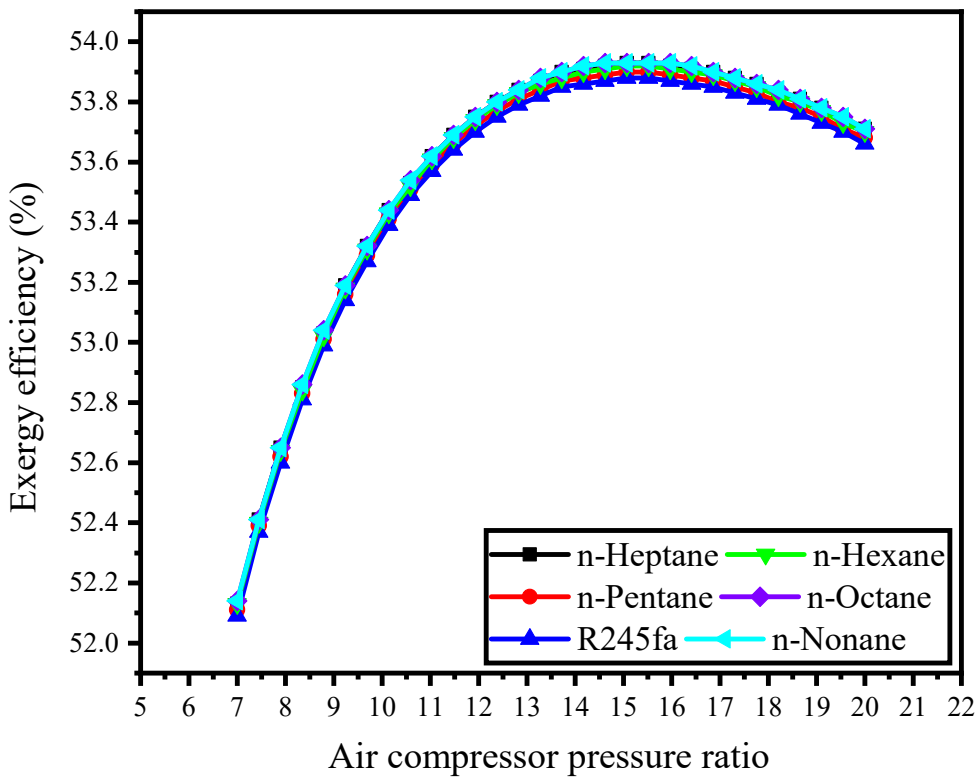

(**c**)

Figure 2. Effects of air compressor pressure ratio on (**a**) *LTE*, (**b**) $\dot{C}_{tot}$, and (**c**) η_{ex} of the combined GT-OFC plant.

Figure 3 shows the effects of the air compressor isentropic efficiency on the system total cost rate, LTE, and exergy efficiency. It is seen that, as η_{AC} rises, η_{ex} of the system increases. If all other decision parameters remain constant, a greater η_{ex} can be achieved because of the higher η_{AC}. However, further increasing of this decision parameter is not cost-effective and results in a rise of $\dot{C}_{tot}$ of the system. The rate of power utilized by the air compressor is reduced by raising η_{AC}, which allows for a decrease in the air mass flow rate. The cost rate related to the gas turbine declines as a result. In the heater, the inlet temperature of the combustion gases rises, which increases the heat transfer rate to the bottoming cycle, and thus the mass flow rate of the working fluid in the OFC increases. In this regard, the net output power generated by the OFC increases, leading to an increase in η_{ex} of the overall system. Bestowing to Equation (11), a growth in the system net output power results in a decrease in LTE. According to Figure 3, the working fluids other than R245fa have almost the same performances and can be used as the working fluid in the OFC.

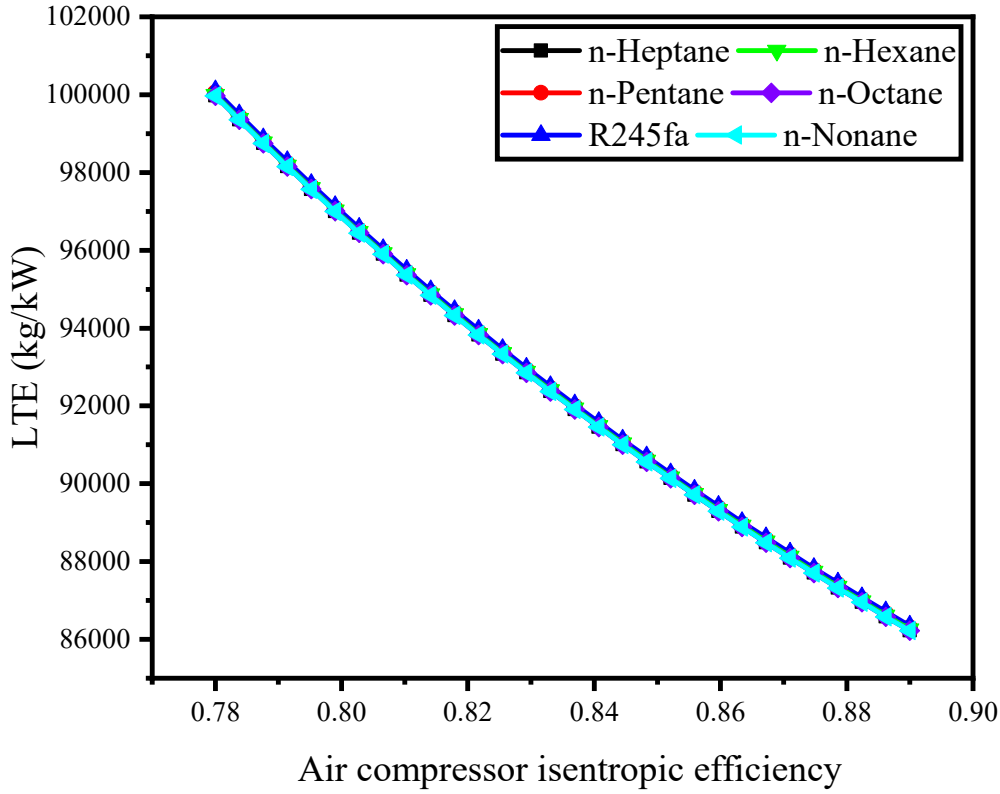

(**a**)

Figure 3. *Cont.*

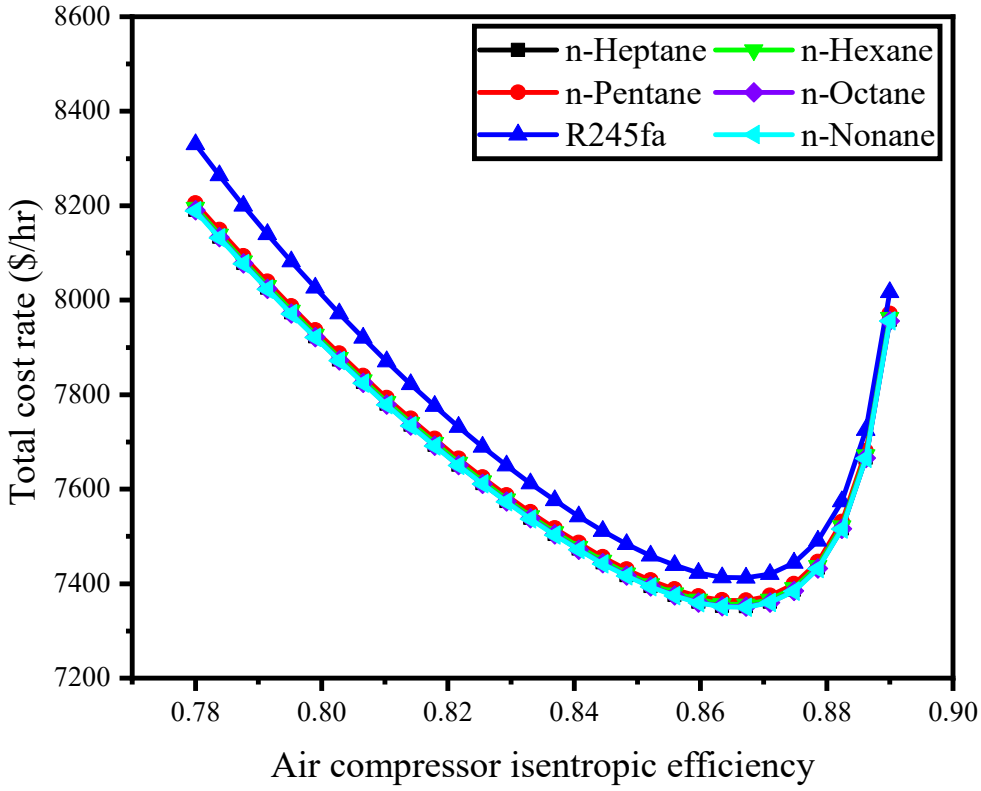

(**b**)

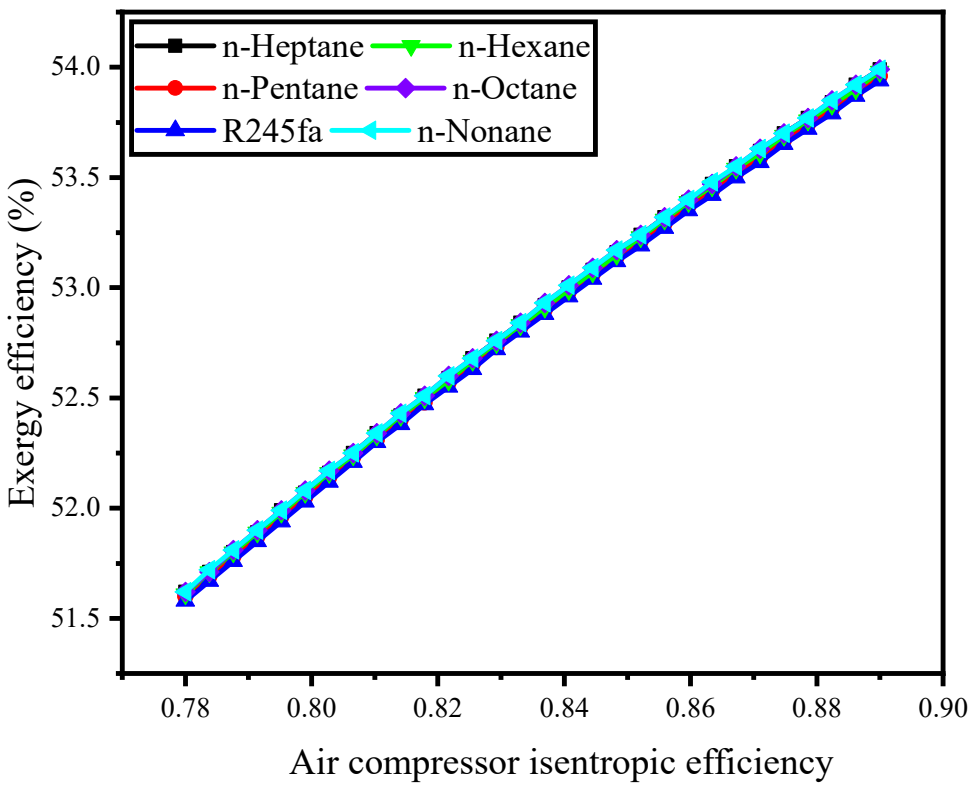

(**c**)

Figure 3. Effects of isentropic efficiency of the air compressor on (**a**) *LTE*, (**b**) $\dot{C}_{tot}$, and (**c**) η_{ex} of the combined GT-OFC plant.

Figure 4 illustrates how the preheated air temperature affects the system LTE, total cost rate, and exergy efficiency. By raising T_3, the system η_{ex} increases, whereas the $\dot{C}_{tot}$ of the system and LTE decrease. Therefore, increasing the preheated air temperature can improve the system performance from environmental, economic, exergy, and energy perspectives. By increasing T_3, the methane mass flow rate declines, and therefore, the heat transfer rate in the combustion chamber decreases. That reduction leads to a drop in the exergy destruction of this component, which, based on Table 12, has the greatest exergy destruction rate. Reducing the destruction of exergy in the combustion chamber raises η_{ex} of the system and causes a reduction in the cost rate of the exergy destruction, reducing $\dot{C}_{tot}$ of the system. n-Octane and n-nonane are seen in Figure 4 to be the best options for use in the OFC from environmental, economic, and thermodynamic perspectives. However, R245fa is not a promising working fluid for the OFC. As a result, a higher air inlet temperature entering the combustion chamber results in better environmental, economic, and thermodynamic performances.

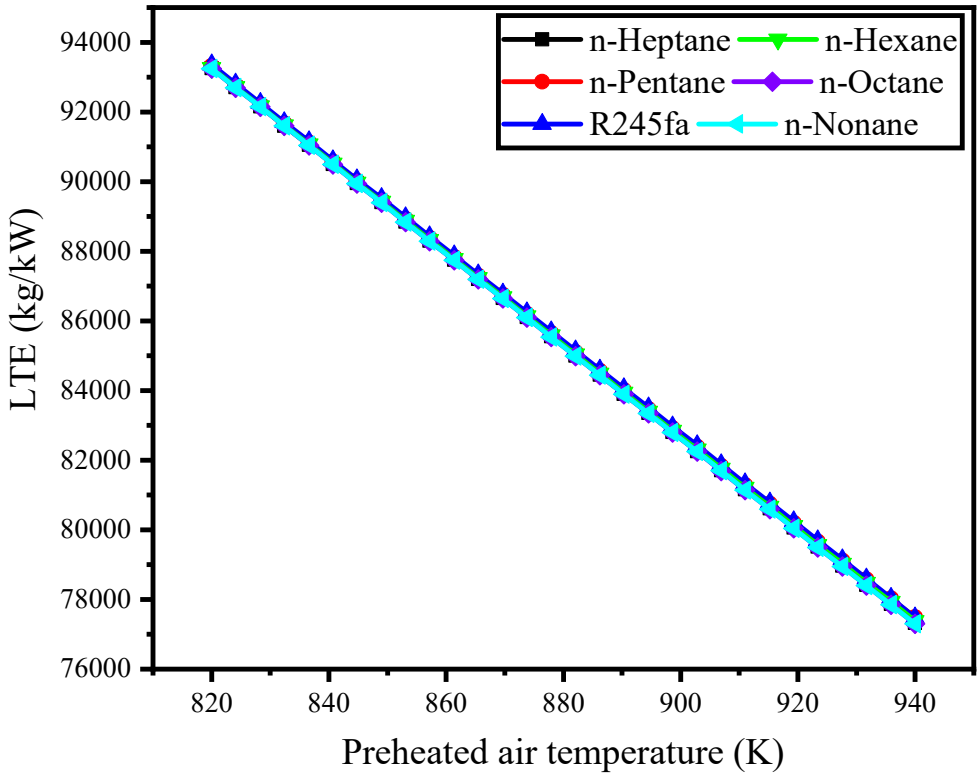

(**a**)

Figure 4. *Cont.*

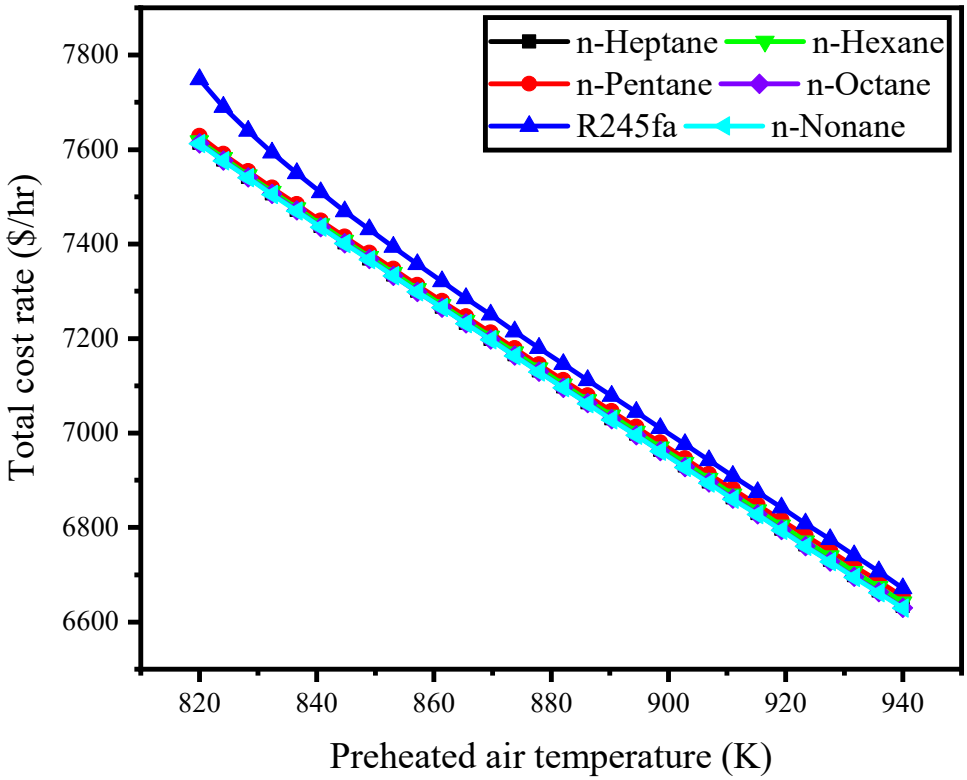

(**b**)

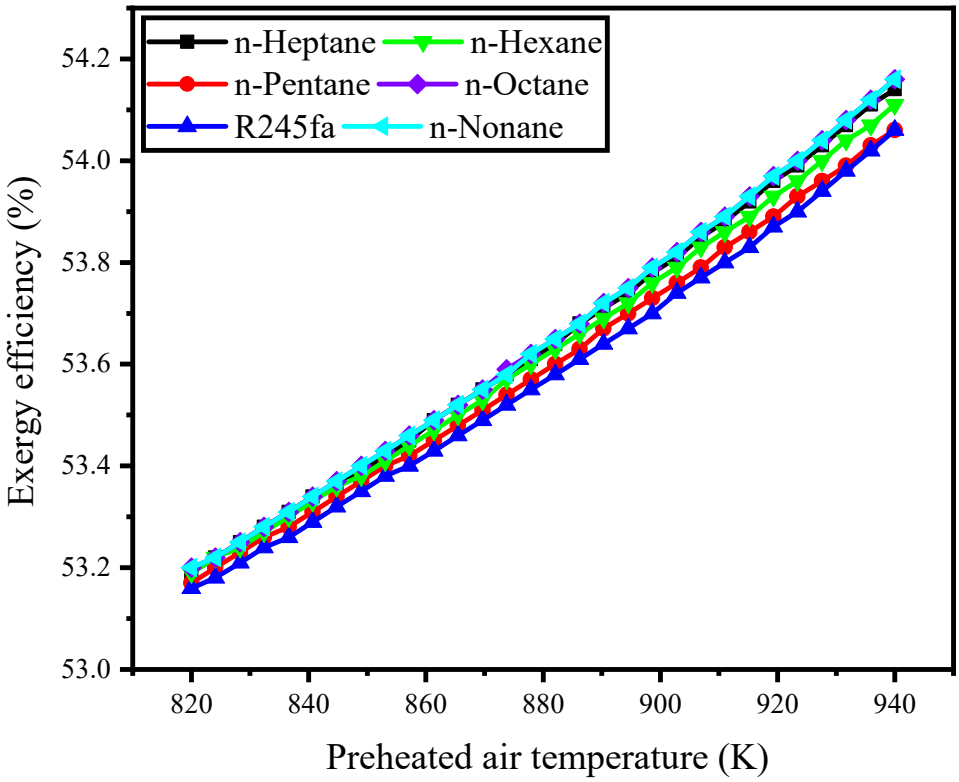

(**c**)

Figure 4. Effects of preheated air temperature on (**a**) *LTE*, (**b**) $\dot{C}_{tot}$, and (**c**) η_{ex} of the combined GT-OFC plant.

The effects of the gas turbine isentropic efficiency on the main three objective functions are illustrated in Figure 5. The effects of η_{GT} and η_{AC} on LTE, $\dot{C}_{tot}$, and η_{ex} of the system exhibit similarities. Specifically, on boosting η_{GT}, η_{ex} rises, but a further increase in η_{GT} does not yield cost-effective results. But by increasing this parameter, LTE and the emission rate of greenhouse gases were reduced. By increasing η_{GT}, the system exergy destruction rate and the rate of consumed methane are reduced, increasing the system efficiency. By increasing η_{GT}, the mass flow rate of fuel is decreased, which reduces the cost rate associated with fuel. However, the investment cost rates of the OFC components increase. As a result, $\dot{C}_{tot}$ of the system is locally minimized. With the exception of R245fa, all working fluids lead to virtually the same performances by increasing η_{GT}.

Figure 6 shows that, as the pinch point temperature difference in the HRSG rises, the system total cost rate and LTE increase, and the system exergy efficiency reduces. Therefore, a lower $\Delta T_{pp,HRSG}$ brings about better system performance. As the specified decision parameter rises, the cost rates associated with capital investment and destruction of exergy in the bottoming cycle increase, which raises $\dot{C}_{tot}$ of the system. The rise in the destruction of exergy of the OFC also increases the overall system's irreversibility and reduces η_{ex} of the combined GT-OFC plant. According to Figure 6, utilization of R245fa as the working fluid leads to the lowest performance from environmental, economic, exergy, and energy perspectives. However, n-nonane and n-octane can be promising working fluids for utilization at the bottoming cycle.

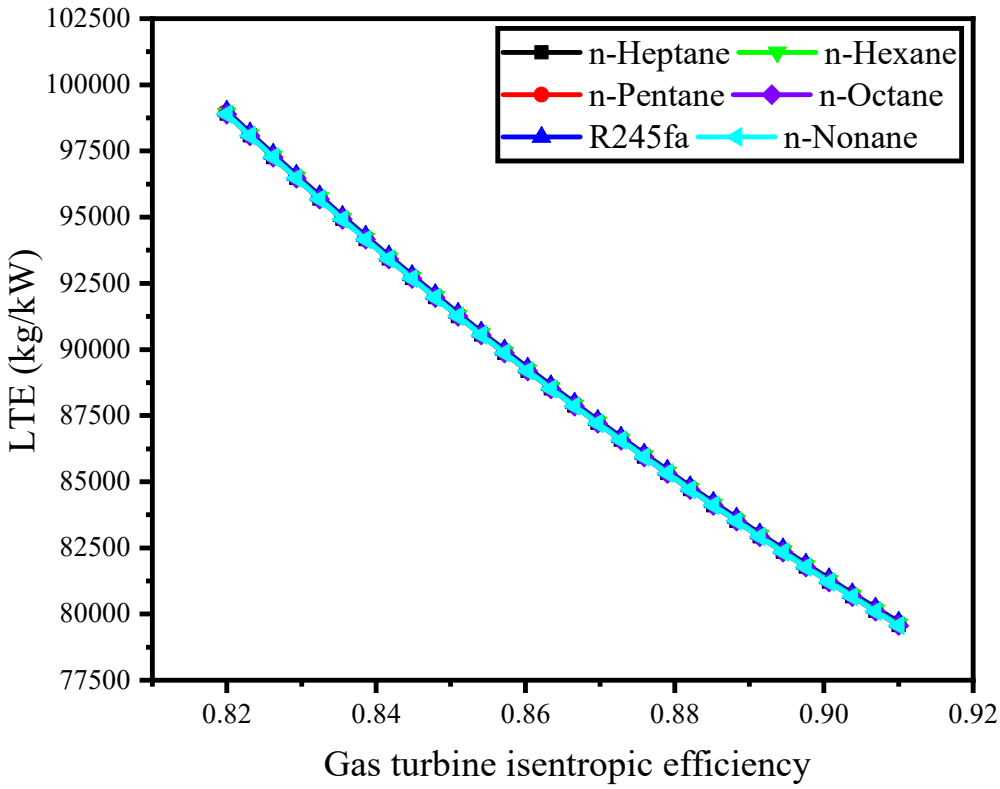

(**a**)

Figure 5. *Cont.*

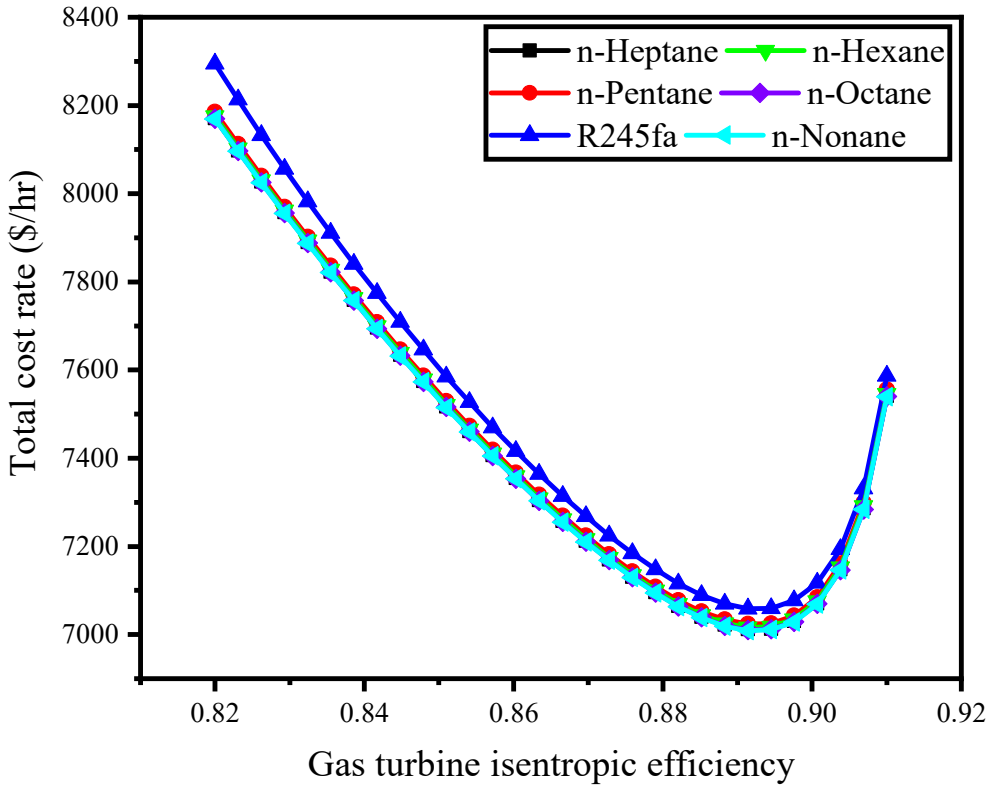

(**b**)

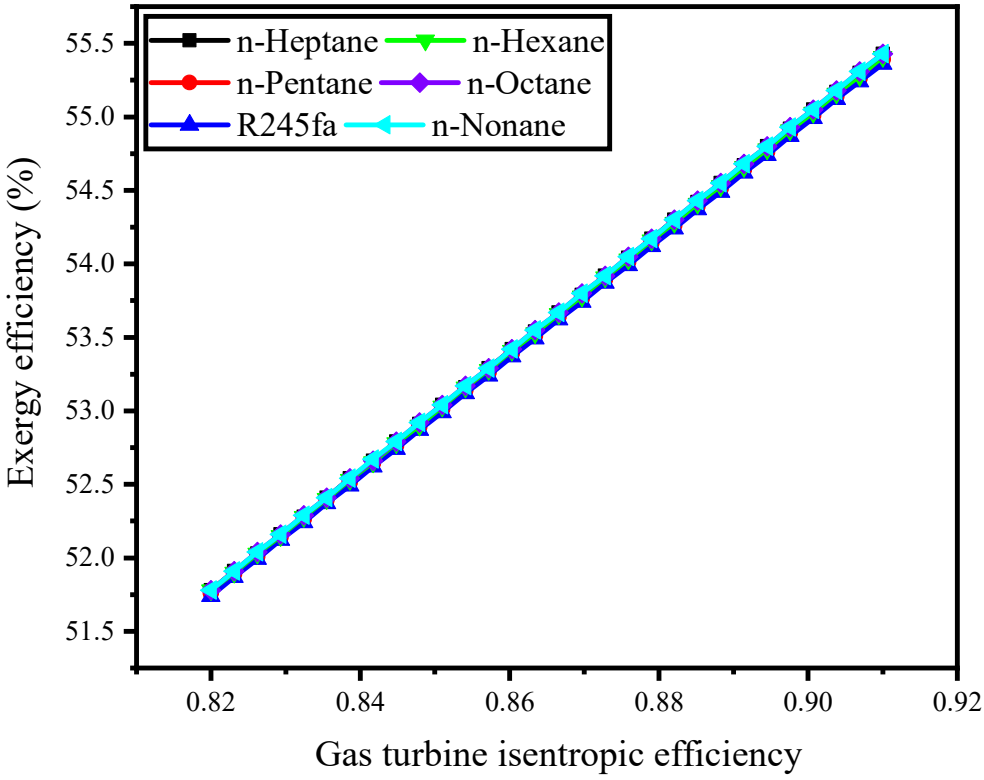

(**c**)

Figure 5. Effects of isentropic efficiency of the gas turbine on (**a**) *LTE*, (**b**) $\dot{C}_{tot}$, and (**c**) η_{ex} of the combined GT-OFC plant.

Figure 7 illustrates the impacts of the terminal temperature difference in the heater on the system LTE, exergy efficiency, and total cost rate. Raising ΔT_{Heater} is not beneficial in terms of environmental impacts, economics, and thermodynamics. Raising ΔT_{Heater} increases LTE and the system's total cost rate and reduces the exergy efficiency. As a result, superior environmental, economic, and thermodynamic performances of the system are achieved when ΔT_{Heater} takes on the feasible possible value. A rise in ΔT_{Heater} causes an increase in the temperature of the combustion gases leaving the heater (state 11), which reduces the heat transfer rate in the heater. In addition, by increasing the mentioned decision variable, the hot combustion gases transfer less heat to the OFC working fluid. By decreasing the exergy heat input to the bottoming cycle, the net output power generated by the OFC decreases and consequently, the combined GT-OFC plant's η_{ex} reduces, while the total investment and operation and maintenance cost rates decrease. The overall system's $\dot{C}_{tot}$ declines because of the notable effect of the reduction of the net output power of the hybrid GT-OFC plant on $\dot{C}_{tot}$. R245fa leads to the lowest performance efficiency among all the working fluids evaluated in this research. Meanwhile, n-octane and n-nonane can be effectively employed in the bottoming cycle.

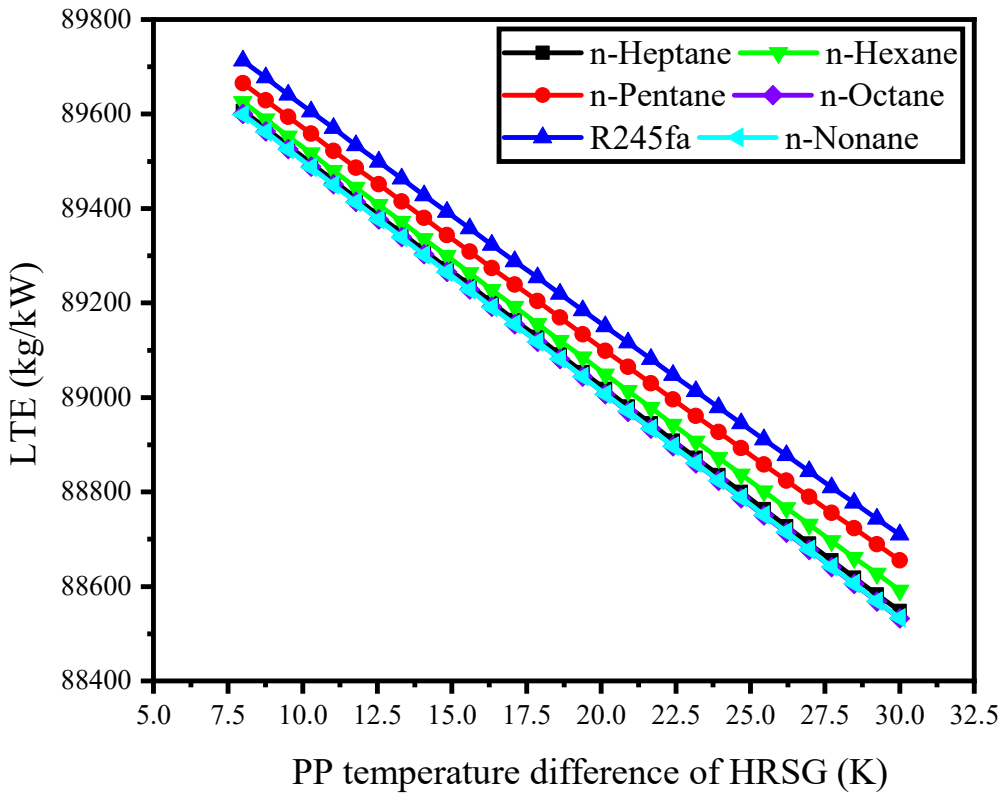

(**a**)

Figure 6. *Cont.*

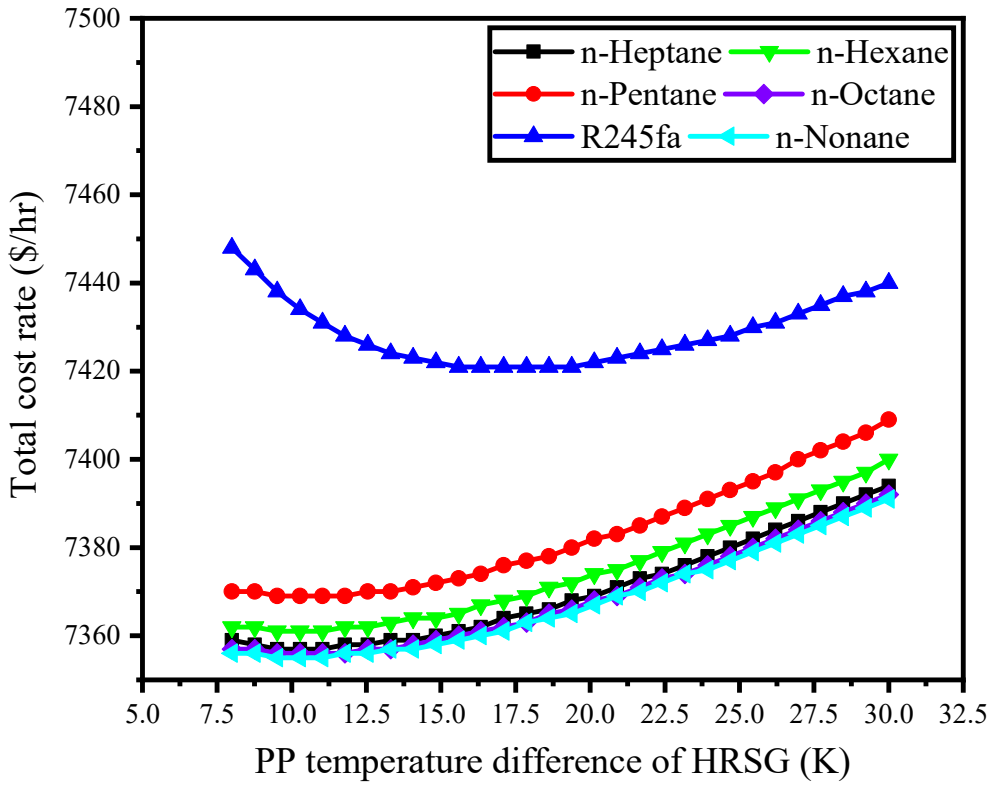

(**b**)

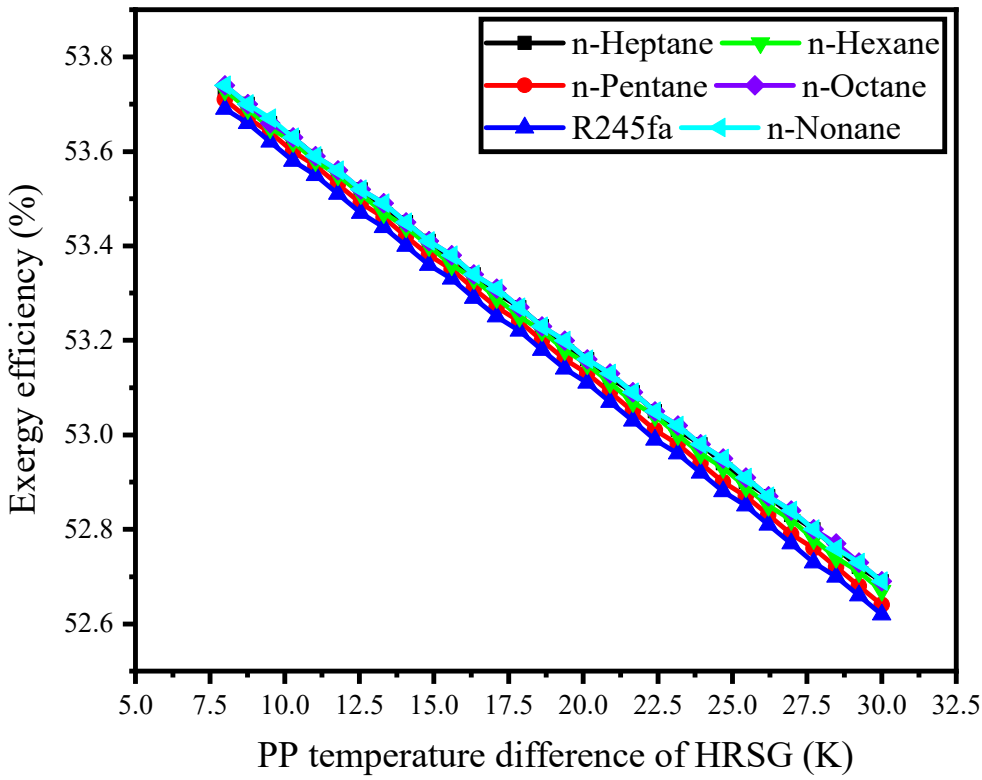

(**c**)

Figure 6. Effects of pinch point temperature difference in the HRSG on (**a**) *LTE*, (**b**) $\dot{C}_{tot}$, and (**c**) η_{ex} of the combined GT-OFC plant.

Figure 8 illustrates how the inlet temperature of the flash separator affects the system LTE, total cost rate, and exergy efficiency. It is seen that, as T_{15} rises, the system η_{ex} is maximized locally, whereas LTE and $\dot{C}_{tot}$ for the system are minimized. Therefore, there should be an optimized value for T_{15} at which η_{ex} takes on the highest possible value and LTE and $\dot{C}_{tot}$ of the system take the lowest possible values. As a result of the unchanged net output power generated in the topping system and the increase in the flash separator inlet temperature, the variations in the three objective functions of the combined GT-OFC plant are just in relation to the performance of the OFC. By raising T_{15}, the inlet pressure and temperature of the turbine (state 16) increase, resulting in a lower working fluid mass flow rate entering the turbine while decreasing the turbine output enthalpy. These modifications result in the lowest and the highest values for the system's $\dot{C}_{tot}$ and η_{ex}, respectively. When n-nonane is used as the working fluid, the combined GT-OFC plant achieves the greatest η_{ex}, the lowest LTE, and the lowest $\dot{C}_{tot}$. Conversely, R245fa has the poorest environmental, economic, and thermodynamic performances.

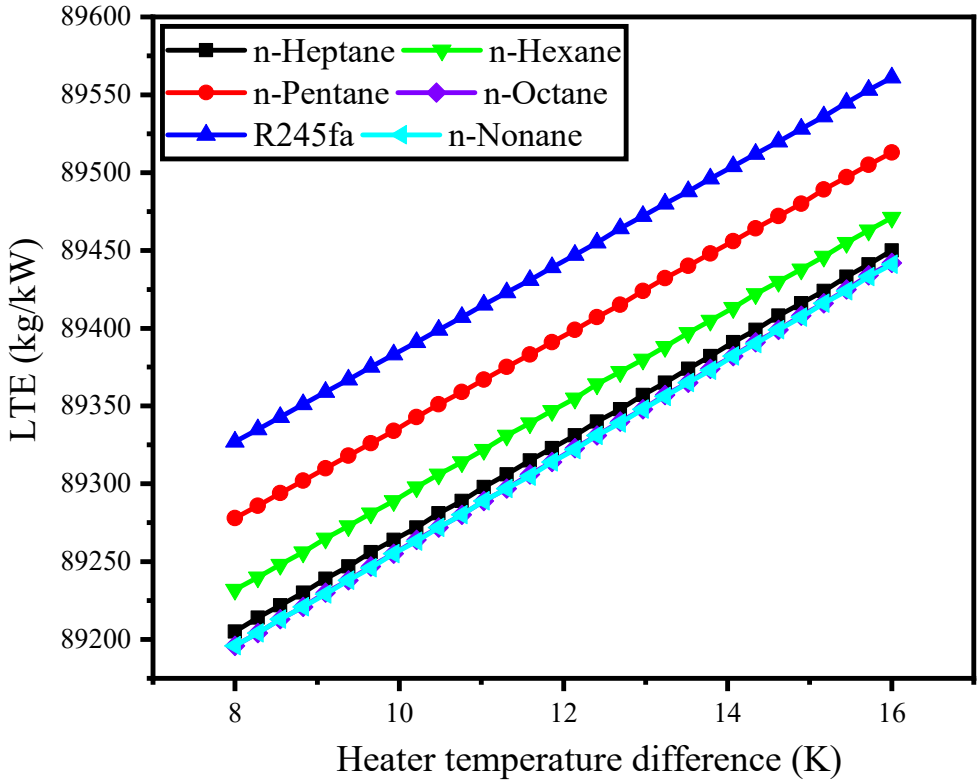

(**a**)

Figure 7. *Cont.*

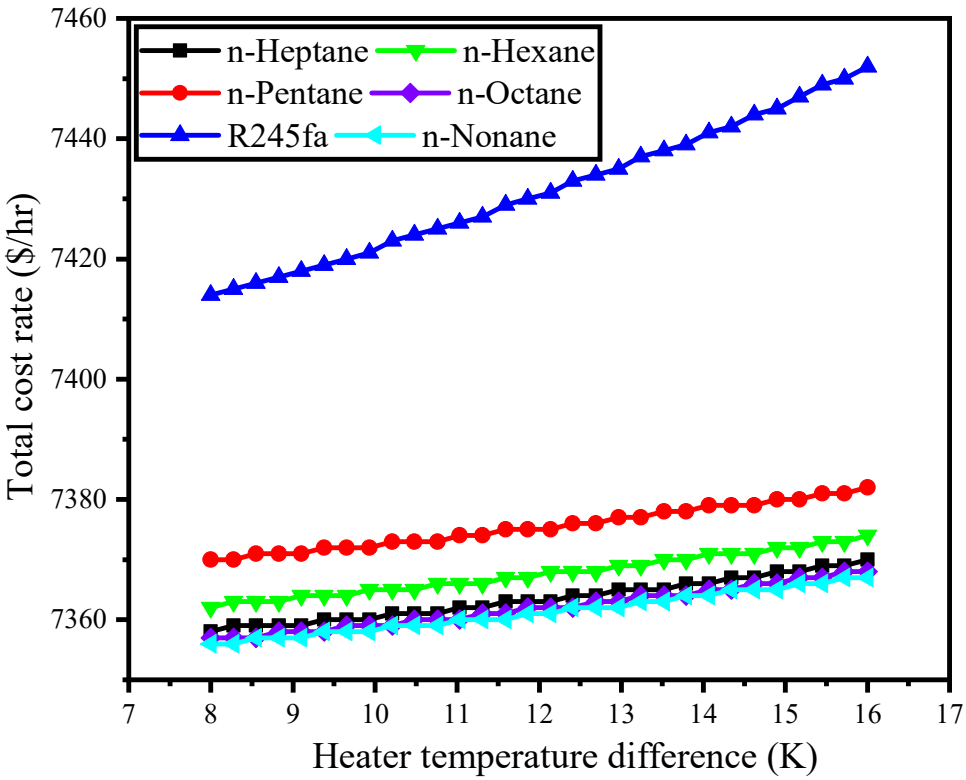

(**b**)

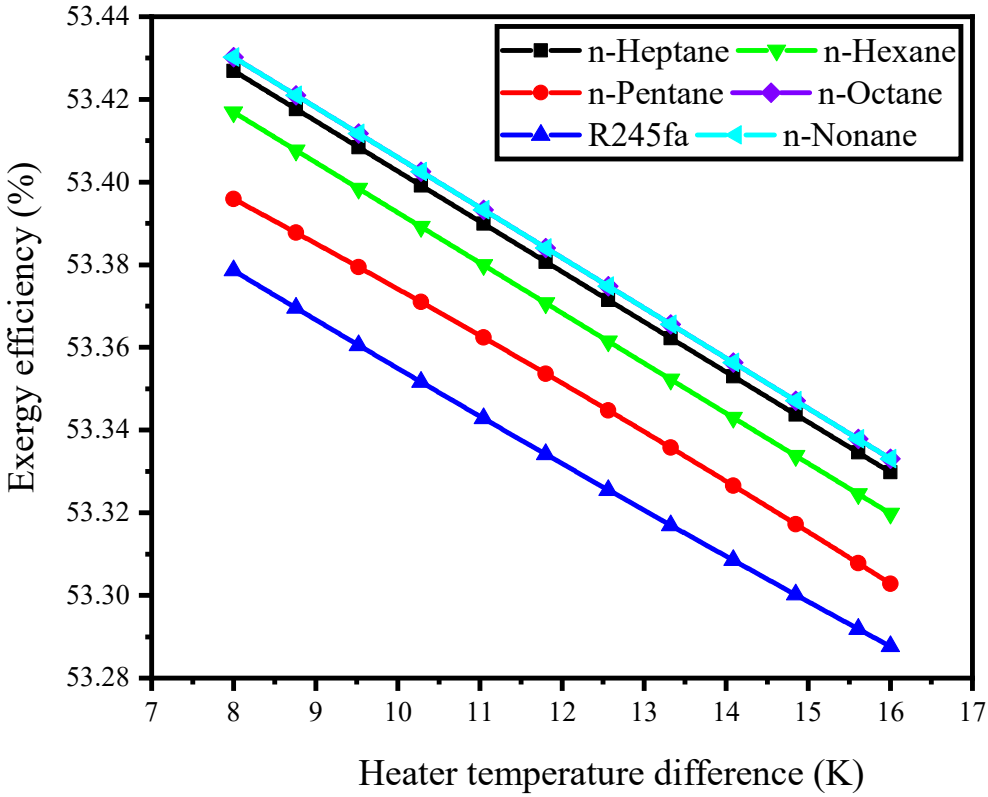

(**c**)

Figure 7. Effects of terminal temperature difference in the heater on (**a**) *LTE*, (**b**) $\dot{C}_{tot}$, and (**c**) η_{ex} of the combined GT-OFC plant.

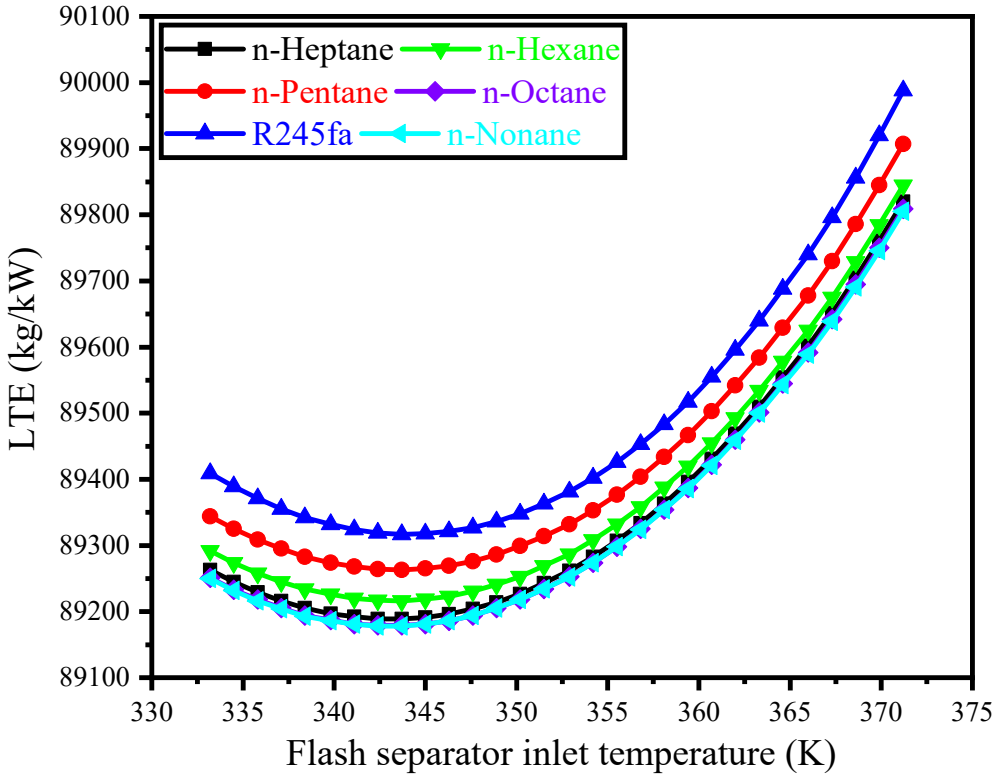

(**a**)

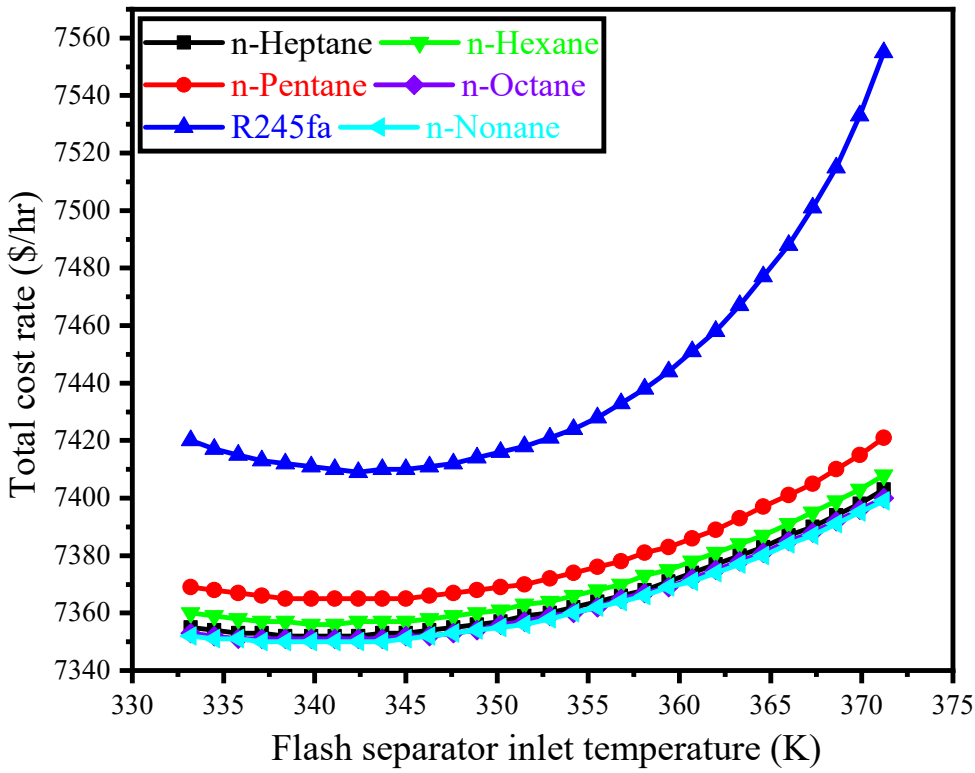

(**b**)

Figure 8. *Cont.*

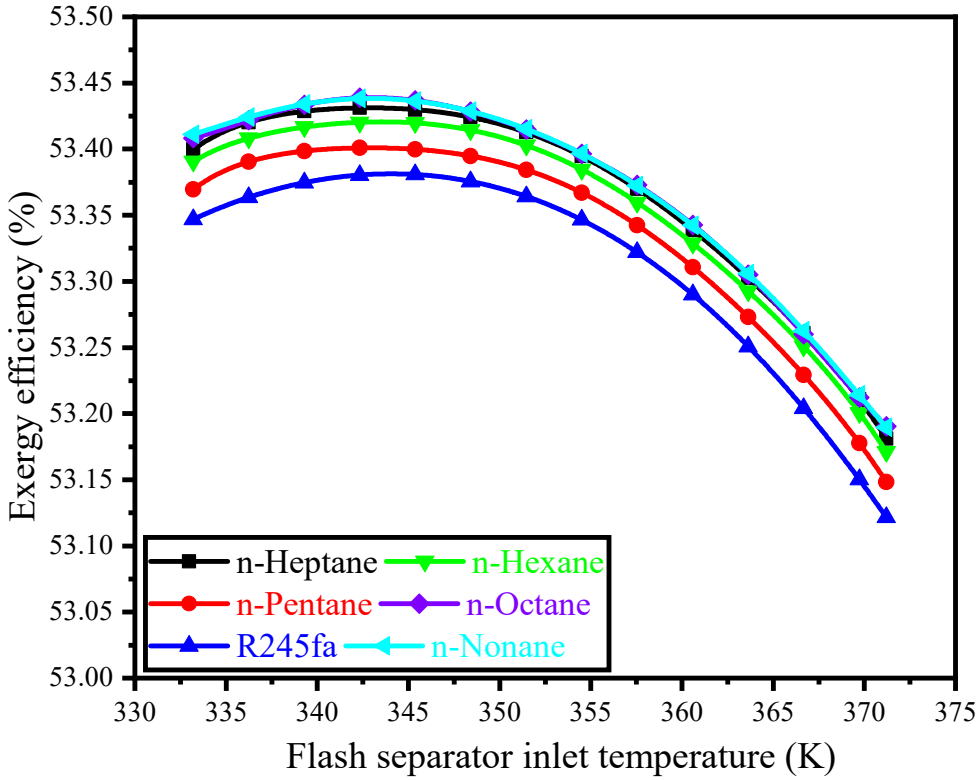

(**c**)

Figure 8. Effects of inlet temperature of the flash separator on (**a**) *LTE*, (**b**) $\dot{C}_{tot}$, and (**c**) η_{ex} of the combined GT-OFC plant.

4.3. Optimization

The analysis of the system's parameters highlights the significant influences of r_{AC}, η_{GT}, η_{AC}, T_3, $\Delta T_{PP,HRSG}$, T_{15}, and ΔT_{Heater} on the performance of the hybrid system. Consequently, these factors have been identified as crucial decision parameters for the optimization processes. To thoroughly optimize the system, four distinct scenarios have been considered: (a) maximizing the system exergy efficiency, (b) minimizing the system total cost rate, (c) minimizing LTE, and (d) multi-objective optimization. The first three scenarios involve optimizations based on single-objective functions while the last involves a multi-objective optimization procedure.

4.3.1. Single-Objective Optimizations (Scenarios a, b, and c)

The optimizations were carried out to maximize the system exergy efficiency, to minimize the total cost rate, or to minimize the LTE. The combined GT-OFC plant optimization was performed using EES software as follows:

For the GT-OFC plant, the maximization of η_{ex} or minimization of $\dot{C}_{tot}$ or minimization of LTE considering the parameters of r_{AC}, η_{GT}, η_{AC}, T_3, $\Delta T_{PP,HRSG}$, T_{15}, and ΔT_{Heater} in the following ranges:

$7 \leq r_{AC} \leq 20$
$81 \leq \eta_{GT}(\%) \leq 91$
$78 \leq \eta_{AC}(\%) \leq 89$
$820 \leq T_3(\mathrm{K}) \leq 940$
$8 \leq \Delta T_{PP,HRSG}(\mathrm{K}) \leq 30$
$333.15 \leq T_{15}(\mathrm{K}) \leq 371.15$
$8 \leq \Delta T_{Heater}(\mathrm{K}) \leq 16$

According to the findings of the parametric study, the highest system exergy efficiency and the lowest system total cost rate and LTE were achieved when n-nonane was utilized as the OFC

working fluid. Therefore, this working fluid is promising, and the results of this working fluid were considered in a multi-objective optimization procedure. Thermodynamic and economic optimizations aim to maximize the system exergy efficiency, minimize the system total cost rate, and minimize the system LTE, respectively. The findings of the environmental, economic, and thermodynamic optimizations are summarized in Table 13.

Table 13. Results of exergy, environmental, and economic optimizations of the integrated GT-OFC plant utilizing n-nonane as the working fluid in the OFC.

Parameter	Base Condition	Maximum η_{ex} (%)	Minimum $\dot{C}_{tot}$ ($/h)	Minimum LTE (kg/kW)
r_{AC}	10	12.18	10.84	12.18
η_{AC} (%)	86	89	86.33	89
T_3 (K)	850	940	940	940
η_{GT} (%)	86	91	89.03	91
$\Delta T_{PP,HRSG}$ (K)	15	8	8	8
ΔT_{Heater} (K)	10	8	8	8
T_{15} (K)	353.15	353.3	365.6	353.2
η_{ex} (%)	53.4	58.2	56.41	58.2
$\dot{C}_{tot}$ ($/h)	7358	8346	6302	8361
LTE (kg/kW)	89,255	64,714	70,726	64,714

According to Table 13, all decision variables, as well as the system LTE, exergy efficiency, and total cost rate, are almost equal for thermodynamic and environmental optimizations, indicating that maximizing the exergy efficiency minimizes the LTE. Therefore, increasing the exergy efficiency enhances the thermodynamic performance of the hybrid GT-OFC system and improves its environmental performance. Furthermore, a higher r_{AC} is necessary to maximize the system exergy efficiency and decrease the total cost rate. According to the findings of the parametric assessment, for maximizing the system exergy efficiency and minimizing the system overall cost rate, $\Delta T_{pp,HRSG}$, and ΔT_{Heater} take on the lowest achievable values, which are 8 K. According to Figures 3 and 5, the optimal exergy efficiency is attained when both η_{AC} and η_{GT} are maximized. However, maximizing η_{AC} and η_{GT} also leads to an increase in the system total cost rate. It is worth noting that the lowest total cost rate of the plant and the greatest exergy efficiency are 16.8% lower and 9.0% higher, respectively, than the combined GT-OFC plant's corresponding values under base conditions. Moreover, the lowest LTE is 64,714 kg/kW, which is 37.9% lower than that of the combined cycle under base design parameters. The only decision variable that remains constant for thermodynamic and economic optimizations is the temperature of the preheated air. This variable is 940 K for all three optimizations.

4.3.2. Multi-Objective Optimization (Scenario d)

After coupling the MATLAB codes with the EES software, the optimization procedure was performed, the PARETO frontier was plotted, and the best performances of the system from environmental, economic, and thermodynamic points of view were achieved. Due to the mentioned reasons, the MOO was performed considering n-nonane as the OFC's working fluid. Figure 9 depicts the PARETO frontier of the MOO.

Table 14 presents the objective functions that are deemed most suitable based on the results obtained from MOO. The table also provides the values of the decision-making variables.

Table 14. Results of MOO considering n-nonane as the OFC working fluid.

Exergy Efficiency	Total Cost Rate	LTE
55%	6873 $/h	74,567 kg/kW

$r_{AC} = 14.28$, $\eta_{GT} = \eta_{AC} = 86$ (%), $T_3 = 939.9$ (K), $\Delta T_{pp,HRSG} = 9.359$ (K), $\Delta T_{Heater} = 11.71$ (K).

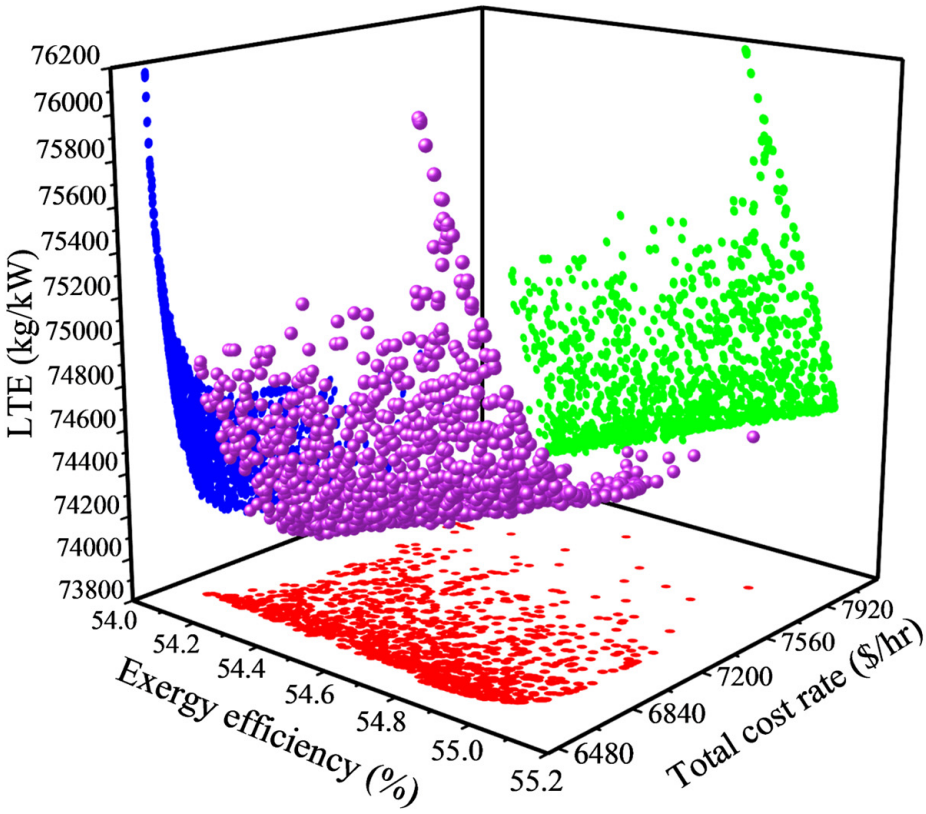

Figure 9. PARETO frontier for the MOO of the combined GT-OFC plant.

Table 15 compares the results of MOO and system under base design conditions. By applying MOO, the power generated by the OFC goes up with 336.1%, which can affect the overall exergy efficiency deeply. Moreover, the system exergy efficiency increases by 3%. Conducting MOO results in better economic performance of the system, which can bring down the system total cost rate by 6.59%. The environmental aspect of the system (LTE) is reduced by 16.45%, which is the highest difference rate among thermodynamic, economic, and environmental aspects. Furthermore, these results indicate that conducting MOO can result in better environmental, thermodynamic, and economic performances.

Table 15. Comparing results of the system under base design conditions and MOO using n-nonane.

Parameter	Results of MOO	Difference (%)
$\dot{W}_{net,tot}$ (kW)	30,667	1.7
$\dot{W}_{OFC}$ (KW)	667.3	336.1
$\eta_{I,GT}$ (%)	55.96	1.7
$\eta_{I,GT-OFC}$ (%)	56.9	3.1
$\eta_{II,GT}$ (%)	54.09	1.7
$\eta_{II,GT-OFC}$ (%)	55	3
$\dot{C}_{tot}$ ($/h)	6873	−6.59
LTE (kg/kW)	74,567	−16.45

Figure 10a–d present the scattered distribution charts for the MOO.

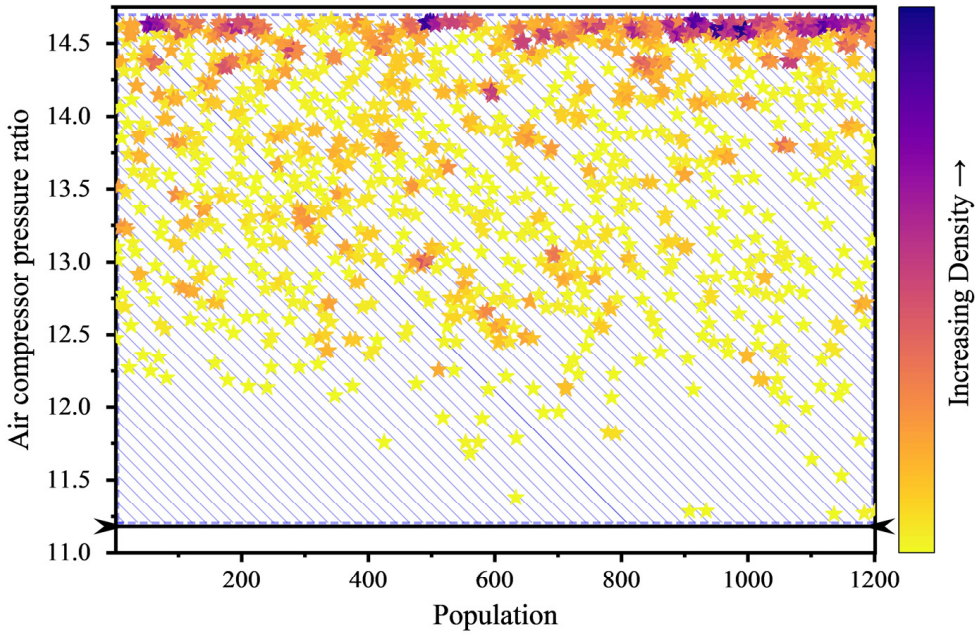

(**a**)

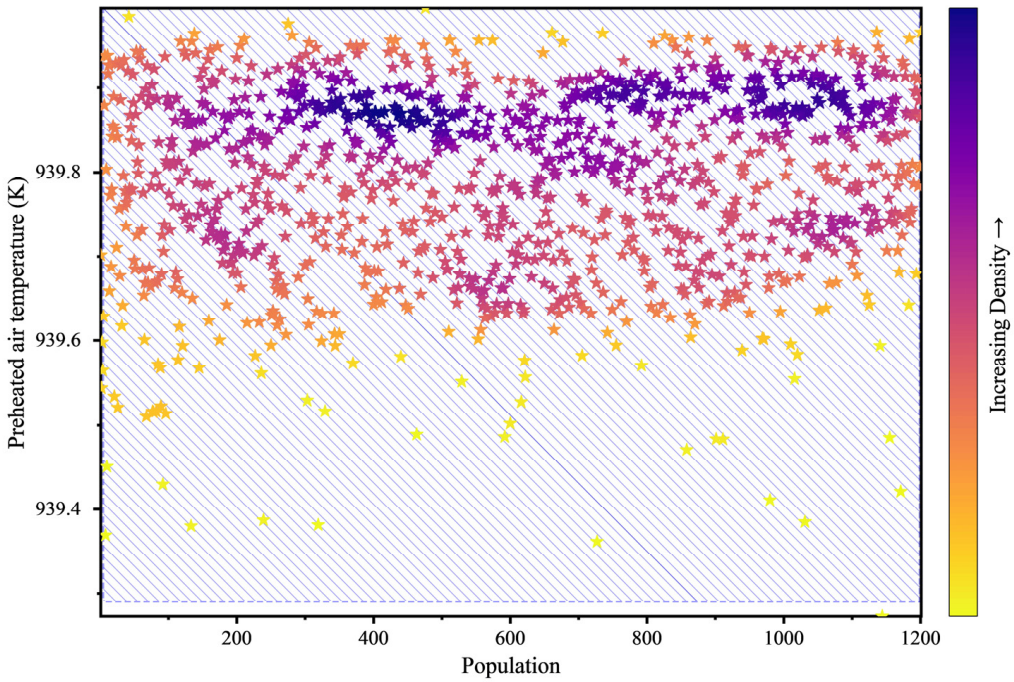

(**b**)

Figure 10. *Cont.*

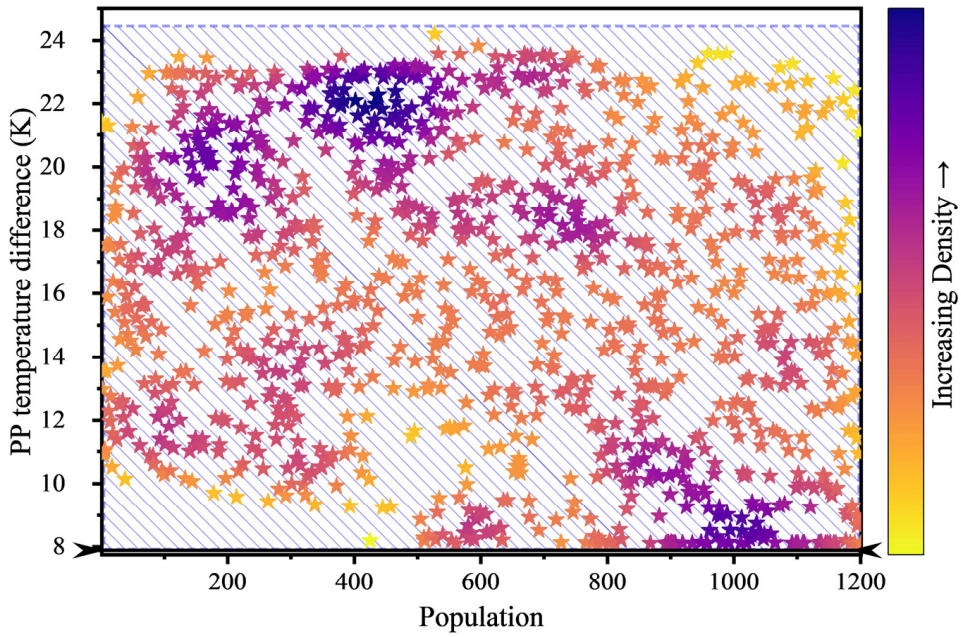

(**c**)

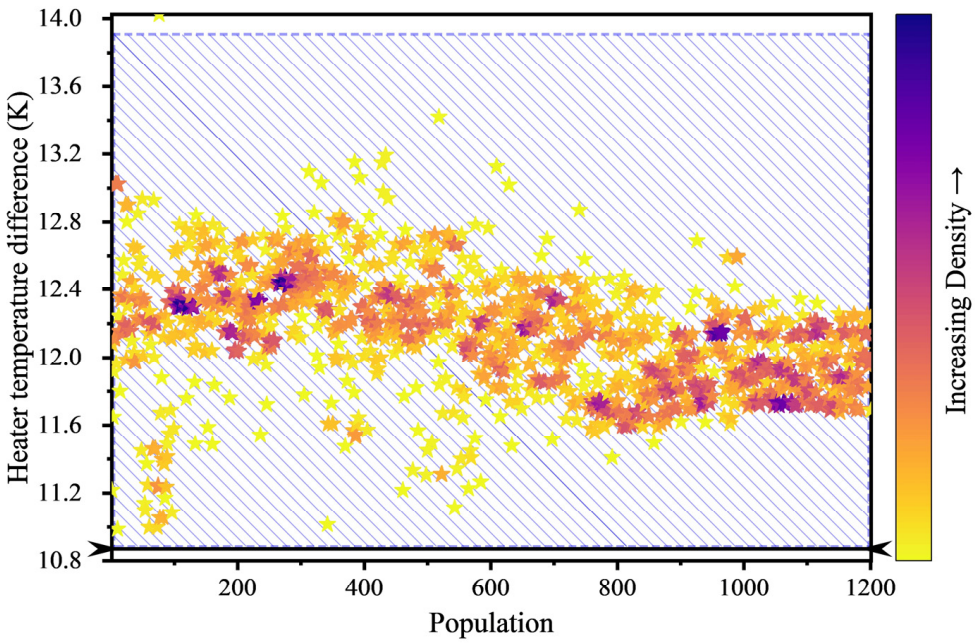

(**d**)

Figure 10. (**a**) Scattered distribution chart for air compressor pressure ratio. (**b**) Scattered distribution chart for preheated air temperature (K). (**c**) Scattered distribution chart for PP temperature difference (K). (**d**) Scattered distribution chart for heater temperature difference (K).

5. Conclusions

The main novelty of the present work was proposing an innovative configuration of combined gas turbine–organic flash cycle (GT-OFC). Also, the main contribution of the research was a comprehensive assessment encompassing environmental, economic, exergy, and energy analyses utilizing six different working fluids in order to assess the plant performance in detail. To explore the impacts of several variables on the system LTE, exergy efficiency, and total cost rate, parametric investigations were performed. The results of the parametric studies revealed that superior environmental, economic, and thermo-

dynamic performances of the integrated GT-OFC plant may be attained with n-nonane utilized as the OFC working fluid. Lastly, the system environmental, economic, and thermodynamic performances were optimized through single- and multi-objective optimizations to minimize the system's overall cost rate and LTE, and to maximize the exergy efficiency. The key findings and conclusions derived from the analyses are listed below:

I. The parametric investigations revealed that the combined GT-OFC plant achieves better thermodynamic, economic, and environmental performances when $\Delta T_{pp,HRSG}$ and ΔT_{Heater} are 8 K, which are the lowest possible values.
II. According to the findings of single-objective optimizations, the maximum exergy efficiency and the lowest LTE were obtained at higher air compressor pressure ratios. However, the system optimal total cost rate was attained at lower pressure ratios.
III. The single-objective optimizations revealed that the lowest total cost rate, the lowest LTE, and the highest exergy efficiency of the system were obtained when the temperature of the preheated air was at its highest possible value of 940 K.
IV. For thermodynamic and environmental single-objective optimizations, the gas turbine and the air compressor isentropic efficiencies and the air compressor pressure ratio were higher than those for the economic optimization. However, the lowest LTE and the highest exergy efficiency attained at lower inlet temperature of the flash separator than that for the system minimum total cost rate.
V. The findings of the thermodynamic and environmental single-objective optimizations demonstrated that the lowest LTE is attained at the highest exergy efficiency, and the values of the variables for both optimizations are virtually the same. Therefore, thermodynamic optimization was nearly equivalent to environmental optimization.
VI. The highest exergy efficiency was determined to be 58.2%, and the lowest total cost rate 6302.4/h for the combined GT-OFC plant. The rate of total cost and exergy efficiency were calculated as 16.8% lower and 9.0% higher, respectively, than those for the GT-OFC plant under base design conditions. In addition, the lowest LTE was 64,714 kg/kW, which was 37.9% lower than that under base design conditions.
VII. According to the results of MOO, the system exergy efficiency, rate of total cost, and the LTE were 55%, 6873 $/h, and 74,569 kg/kW, respectively.
VIII. Among the six distinct working fluids considered, n-nonane achieved the best environmental, economic, and thermodynamic performances based on the parametric analyses. From a technical aspect, the main reason is that n-nonane has the highest and the lowest critical temperature and critical pressure, respectively. Moreover, this fluid has zero environmental impact. Therefore, this fluid can be an excellent choice as the working fluid in the combined GT-OFC plant.
IX. The highest cost of exergy destruction and the exergy destruction rate was achieved in the combustion chamber accounting for 60.06% and 68.97% of the overall system, respectively. Thus, this component played a major role in the system environmental, economic, and thermodynamic performances.

Future research can compare different bottoming cycles, encompassing ORC, Kalina cycle, and supercritical CO_2 cycle, combined with the GT system from environmental, economic, exergy, and energy aspects to determine the most appropriate plant. Moreover, advanced exergy and exergo-economic analyses can be applied to the GT-OFC system to enhance its thermodynamic and economic performances.

Author Contributions: R.G.S., A.J.: Methodology, Software, Validation, Formal analysis, Writing—original draft; S.M.S.M.: Conceptualization, Supervision, Validation; M.A.K.: Methodology, Writing—review & editing; M.A.R.: Conceptualization, Supervision, Validation. All authors have read and agreed to the published version of the manuscript.

Funding: This research received no external funding.

Institutional Review Board Statement: Not applicable.

Informed Consent Statement: Not applicable.

Data Availability Statement: The data presented in this study are available on request from the corresponding author.

Conflicts of Interest: The authors declare that they have no known competing financial interests or personal relationships that could have appeared to influence the work reported in this paper.

Nomenclature

Symbols		γ	Maintenance factor
A	Area (m^2)	τ	Residence time (s)
$\dot{C}$	Cost rate ($/h)	ΔT	Temperature difference (K)
c	Average cost per unit exergy ($/GJ)	*Superscripts*	
CH_4	Methane	CI	Capital investment
CRF	Capital recovery factor	OM	Operation and maintenance
$\dot{E}$	Exergy rate (MW)	*Subscripts*	
$\bar{e}$	Specific molar exergy (kJ/kmol)	0	Ambient condition
f	Exergo-economic factor (%)	1, 2, etc.	State points
h	Specific enthalpy (kJ/kg)	APH	Air preheater
H_2O	Water	AC	Air compressor
i_r	Interest rate (%)	CO_2	Carbon dioxide
ΔT_{LMTD}	Logarithmic mean temperature difference (K)	CC	Combustion chamber
LHV	Lower heating value (kJ/kmol)	ch	Chemical
LTE	Levelized total emission (kg/kW)	CO	Carbon monoxide
$\dot{m}$	Mass flow rate (kg/s)	Comb.gases	Combustion gases
m	Greenhouse gas mass ratio ($g_{pollutant}/kg_{fuel}$)	Cond	Condenser
MOO	Multi-objective optimization	D	Destruction
$\dot{n}$	Molar flow rate (kmol/s)	env	Environmental
N	Number of operation years	ex	Exergy
N_2	Nitrogen	f	Fuel
O_2	Oxygen	FS	Flash separator
P	Pressure (bar)	GT	Gas turbine
$\dot{Q}$	Heat transfer rate (MW)	HRSG	Heat recovery steam generator
r	Pressure ratio	in	Inlet
$\bar{R}$	Universal gas constant (8.314 kJ/kmol.K)	L	Loss
S	Specific entropy (kJ/kg.K)	NOx	Nitrogen oxide
t	Annual plant operation hours	out	Outlet
T	Temperature (K)	P	Pump
U	Overall heat transfer coefficient ($kW/m^2.K$)	ph	Physical
$\dot{W}$	Produced/consumed power (MW)	PP	Pinch point
X	Molar fraction	Pz	Primary zone of combustion chamber
Z	Capital investment cost ($)	T	Turbine
$\dot{Z}$	Capital investment cost rate ($/h)	th	Thermal
Greek symbols		tot	Total
η	Efficiency (%)	V	Valve

References

1. Ahmadi, B.; Golneshan, A.A.; Arasteh, H.; Karimipour, A.; Bach, Q.-V. Energy and Exergy Analysis and Optimization of a Gas Turbine Cycle Coupled by a Bottoming Organic Rankine Cycle. *J. Therm. Anal. Calorim.* **2020**, *141*, 495–510. [CrossRef]
2. Köse, Ö.; Koç, Y.; Yağlı, H. Energy, Exergy, Economy and Environmental (4E) Analysis and Optimization of Single, Dual and Triple Configurations of the Power Systems: Rankine Cycle/Kalina Cycle, Driven by a Gas Turbine. *Energy Convers. Manag.* **2021**, *227*, 113604. [CrossRef]
3. Panwar, N.L.; Kaushik, S.C.; Kothari, S. Role of Renewable Energy Sources in Environmental Protection: A Review. *Renew. Sustain. Energy Rev.* **2011**, *15*, 1513–1524. [CrossRef]
4. Salame, C.; Aillerie, M.; Papageorgas, P. The International Conference on Technologies and Materials for Renewable Energy, Environment and Sustainability. *Energy Procedia* **2015**, *74*, 1–3. [CrossRef]
5. Aigba, P.; Emovon, I.; Samuel, O.; Enweremadu, C.; Abdeljawad, T.; Al-Mdallal, Q.; Afzal, A. Exergetic Assessment of Waste Gas to Energy in a Novel Integrated NGL Recovery and Power Generation Plant. *Front. Energy Res.* **2022**, *9*, 798896. [CrossRef]

6. Crespi, F.; Gavagnin, G.; Sánchez, D.; Martínez, G.S. Supercritical Carbon Dioxide Cycles for Power Generation: A Review. *Appl. Energy* **2017**, *195*, 152–183. [CrossRef]
7. El-Suleiman, A.; Samuel, O.D.; Amosun, S.T.; Emovon, I.; Ashiedu, F.I.; Fayomi, O.S.I.; Layeni, A.; Nwaokocha, C.N.; Afolalu, S.A. Gas Turbine Performance Forecast and Assessment: GE LM2500 in Outlook. *IOP Conf. Ser. Mater. Sci. Eng.* **2021**, *1107*, 12025. [CrossRef]
8. Javaherian, A.; Ghasemzadeh, N.; Javanshir, N.; Yari, M.; Vajdi, M.; Nami, H. Techno-Environmental Assessment and Machine Learning-Based Optimization of a Novel Dual-Source Multi-Generation Energy System. *Process Saf. Environ. Prot.* **2023**, *176*, 537–559. [CrossRef]
9. Aminov, Z.; Nakagoshi, N.; Xuan, T.D.; Higashi, O.; Alikulov, K. Evaluation of the Energy Efficiency of Combined Cycle Gas Turbine. Case Study of Tashkent Thermal Power Plant, Uzbekistan. *Appl. Therm. Eng.* **2016**, *103*, 501–509. [CrossRef]
10. Baina, F.; Malmquist, A.; Alejo, L.; Fransson, T.H. Effect of the Fuel Type on the Performance of an Externally Fired Micro Gas Turbine Cycle. *Appl. Therm. Eng.* **2015**, *87*, 150–160. [CrossRef]
11. Heppenstall, T. Advanced Gas Turbine Cycles for Power Generation: A Critical Review. *Appl. Therm. Eng.* **1998**, *18*, 837–846. [CrossRef]
12. Su, R.; Yu, Z.; Xia, L.; Sun, J. Performance Analysis and Multi-Objective Optimization of an Integrated Gas Turbine/Supercritical CO2 Recompression/Transcritial CO_2 Cogeneration System Using Liquefied Natural Gas Cold Energy. *Energy Convers. Manag.* **2020**, *220*, 113136. [CrossRef]
13. Poullikkas, A. An Overview of Current and Future Sustainable Gas Turbine Technologies. *Renew. Sustain. Energy Rev.* **2005**, *9*, 409–443. [CrossRef]
14. Valero, A.; Lozano, M.A.; Serra, L.; Tsatsaronis, G.; Pisa, J.; Frangopoulos, C.; von Spakovsky, M.R. CGAM Problem: Definition and Conventional Solution. *Energy* **1994**, *19*, 279–286. [CrossRef]
15. Frangopoulos, C.A. Application of the Thermoeconomic Functional Approach to the CGAM Problem. *Energy* **1994**, *19*, 323–342. [CrossRef]
16. von Spakovsky, M.R. Application of Engineering Functional Analysis to the Analysis and Optimization of the CGAM Problem. *Energy* **1994**, *19*, 343–364. [CrossRef]
17. Singhal, S.C. Solid Oxide Fuel Cells for Stationary, Mobile, and Military Applications. *Solid State Ionics* **2002**, *152*, 405–410. [CrossRef]
18. Giampaolo, T. *Gas Turbine Handbook: Principles and Practice*, 5th ed.; River Publishers: Copenhagen, Denmark, 2020; ISBN 9788770223133.
19. Binotti, M.; De Giorgi, P.; Sanchez, D.; Manzolini, G. Comparison of Different Strategies for Heliostats Aiming Point in Cavity and External Tower Receivers. *J. Sol. Energy Eng.* **2016**, *138*, 4032450. [CrossRef]
20. Ibrahim, T.K.; Mohammed, M.K.; Abdulrazzaq Al Door, W.H.; Al-Sammarraie, A.T.; Basrawi, F. Study of The Performance of The Gas Turbine Power Plants from The Simple To Complex Cycle: A Technical Review. *J. Adv. Res. Fluid Mech. Therm. Sci.* **2020**, *57*, 228–250.
21. Ameri, M.; Enadi, N. Thermodynamic Modeling and Second Law Based Performance Analysis of a Gas Turbine Power Plant (Exergy and Exergoeconomic Analysis). *J. Power Technol.* **2012**, *92*, 2012.
22. Pirkandi, J.; Maroufi, A.; Khodaparast, S. Parametric Simulation and Performance Analysis of a Solar Gas Turbine Power Plant from Thermodynamic and Exergy Perspectives. *J. Mech. Sci. Technol.* **2018**, *32*, 2365–2375. [CrossRef]
23. Barzegar Avval, H.; Ahmadi, P.; Ghaffarizadeh, A.R.; Saidi, M.H. Thermo-Economic-Environmental Multiobjective Optimization of a Gas Turbine Power Plant with Preheater Using Evolutionary Algorithm. *Int. J. Energy Res.* **2011**, *35*, 389–403. [CrossRef]
24. Altinkaynak, M.; Ozturk, M. Thermodynamic Analysis of a Novel Integrated System Operating with Gas Turbine, s-CO_2 and t-CO_2 Power Systems for Hydrogen Production and Storage. *Int. J. Hydrogen Energy* **2022**, *47*, 3484–3503. [CrossRef]
25. Maroufi, A.; Pirkandi, J.; Ommian, M. Exergy and Economic Investigation of Different Strategies of Hybrid Systems Consisting of Gas Turbine (GT) and Solid Oxide Fuel Cell (SOFC). *Int. J. Integr. Eng.* **2022**, *14*, 127–139.
26. Liu, X.; Zeng, Z.; Hu, G.; Asgari, A. Thermodynamic, Environmental, and Economic Analysis of a Novel Power and Water Production System Driven by Gas Turbine Cycle. *Alexandria Eng. J.* **2022**, *61*, 9529–9551. [CrossRef]
27. Du, J.; Guo, J.; Zhang, Z.; Li, M.; Ren, F.; Liu, Y. A Triple Cascade Gas Turbine Waste Heat Recovery System Based on Supercritical CO2 Brayton Cycle: Thermal Analysis and Optimization. *Energy Convers. Manag. X* **2022**, *16*, 100297. [CrossRef]
28. Tchanche, B.F.; Lambrinos, G.; Frangoudakis, A.; Papadakis, G. Low-Grade Heat Conversion into Power Using Organic Rankine Cycles—A Review of Various Applications. *Renew. Sustain. Energy Rev.* **2011**, *15*, 3963–3979. [CrossRef]
29. Bianchi, M.; De Pascale, A. Bottoming Cycles for Electric Energy Generation: Parametric Investigation of Available and Innovative Solutions for the Exploitation of Low and Medium Temperature Heat Sources. *Appl. Energy* **2011**, *88*, 1500–1509. [CrossRef]
30. Nemati, A.; Nami, H.; Ranjbar, F.; Yari, M. A Comparative Thermodynamic Analysis of ORC and Kalina Cycles for Waste Heat Recovery: A Case Study for CGAM Cogeneration System. *Case Stud. Therm. Eng.* **2017**, *9*, 1–13. [CrossRef]
31. Khaljani, M.; Khoshbakhti Saray, R.; Bahlouli, K. Comprehensive Analysis of Energy, Exergy and Exergo-Economic of Cogeneration of Heat and Power in a Combined Gas Turbine and Organic Rankine Cycle. *Energy Convers. Manag.* **2015**, *97*, 154–165. [CrossRef]
32. Mohammadi, A.; Kasaeian, A.; Pourfayaz, F.; Ahmadi, M.H. Thermodynamic Analysis of a Combined Gas Turbine, ORC Cycle and Absorption Refrigeration for a CCHP System. *Appl. Therm. Eng.* **2017**, *111*, 397–406. [CrossRef]
33. Cao, Y.; Gao, Y.; Zheng, Y.; Dai, Y. Optimum Design and Thermodynamic Analysis of a Gas Turbine and ORC Combined Cycle with Recuperators. *Energy Convers. Manag.* **2016**, *116*, 32–41. [CrossRef]
34. Ahmadi, P.; Dincer, I.; Rosen, M.A. Exergo-Environmental Analysis of an Integrated Organic Rankine Cycle for Trigeneration. *Energy Convers. Manag.* **2012**, *64*, 447–453. [CrossRef]
35. Hemadri, V.B.; Subbarao, P.M. V Thermal Integration of Reheated Organic Rankine Cycle (RH-ORC) with Gas Turbine Exhaust for Maximum Power Recovery. *Therm. Sci. Eng. Prog.* **2021**, *23*, 100876. [CrossRef]

36. Sun, L.; Wang, D.; Xie, Y. Thermodynamic and Exergoeconomic Analysis of Combined Supercritical CO2 Cycle and Organic Rankine Cycle Using CO_2-Based Binary Mixtures for Gas Turbine Waste Heat Recovery. *Energy Convers. Manag.* **2021**, *243*, 114400. [CrossRef]
37. Ancona, M.; Bianchi, M.; Branchini, L.; Pascale, A.; Melino, F.; Peretto, A.; Torricelli, N. A Comparison Between ORC and Supercritical CO_2 Bottoming Cycles for Energy Recovery From Industrial Gas Turbines Exhaust Gas. *J. Eng. Gas Turbines Power* **2021**, *143*, 4051950. [CrossRef]
38. Pan, M.; Chen, X.; Li, X. Multi-Objective Analysis and Optimization of Cascade Supercritical CO_2 Cycle and Organic Rankine Cycle Systems for Waste-to-Energy Power Plant. *Appl. Therm. Eng.* **2022**, *214*, 118882. [CrossRef]
39. Baccioli, A.; Antonelli, M. Organic Flash Cycles: Off-Design Behavior and Control Strategies of Two Different Cycle Architectures for Waste Heat Recovery Applications. *Energy Convers. Manag.* **2018**, *157*, 176–185. [CrossRef]
40. Ding, P.; Liu, X.; Qi, H.; Shen, H.; Liu, X.; Farkoush, S.G. Multi-Objective Optimization of a New Cogeneration System Driven by Gas Turbine Cycle for Power and Freshwater Production. *J. Clean. Prod.* **2021**, *288*, 125639. [CrossRef]
41. Zhang, B.; Chen, Y.; Wang, Z.; Shakibi, H. Thermodynamic, Environmental, and Optimization of a New Power Generation System Driven by a Gas Turbine Cycle. *Energy Rep.* **2020**, *6*, 2531–2548. [CrossRef]
42. Ebrahimi-Moghadam, A.; Moghadam, A.J.; Farzaneh-Gord, M.; Aliakbari, K. Proposal and Assessment of a Novel Combined Heat and Power System: Energy, Exergy, Environmental and Economic Analysis. *Energy Convers. Manag.* **2020**, *204*, 112307. [CrossRef]
43. Ji-chao, Y.; Sobhani, B. Integration of Biomass Gasification with a Supercritical CO2 and Kalina Cycles in a Combined Heating and Power System: A Thermodynamic and Exergoeconomic Analysis. *Energy* **2021**, *222*, 119980. [CrossRef]
44. Ebrahimi-Moghadam, A.; Farzaneh-Gord, M.; Jabari Moghadam, A.; Abu-Hamdeh, N.H.; Lasemi, M.A.; Arabkoohsar, A.; Alimoradi, A. Design and Multi-Criteria Optimisation of a Trigeneration District Energy System Based on Gas Turbine, Kalina, and Ejector Cycles: Exergoeconomic and Exergoenvironmental Evaluation. *Energy Convers. Manag.* **2021**, *227*, 113581. [CrossRef]
45. Liu, Z.; Ehyaei, M.A. Thermoeconomic and Exergoenvironmental Assessments of a Combined Micro-Gas Turbine and Superheated Kalina Cycles for Cogeneration of Heat and Electrical Power Using Biomass. *Int. J. Environ. Sci. Technol.* **2022**, *19*, 11233–11248. [CrossRef]
46. Yari, M.; Mehr, A.S.; Zare, V.; Mahmoudi, S.M.S.; Rosen, M.A. Exergoeconomic Comparison of TLC (Trilateral Rankine Cycle), ORC (Organic Rankine Cycle) and Kalina Cycle Using a Low Grade Heat Source. *Energy* **2015**, *83*, 712–722. [CrossRef]
47. Bianchi, G.; Kennedy, S.; Zaher, O.; Tassou, S.A.; Miller, J.; Jouhara, H. Numerical Modeling of a Two-Phase Twin-Screw Expander for Trilateral Flash Cycle Applications. *Int. J. Refrig.* **2018**, *88*, 248–259. [CrossRef]
48. Wang, Q.; Wu, W.; Li, D.; Wang, J.; He, Z. Thermodynamic Analysis and Optimization of Four Organic Flash Cycle Systems for Waste Heat Recovery. *Energy Convers. Manag.* **2020**, *221*, 113171. [CrossRef]
49. Ho, T.; Mao, S.S.; Greif, R. Comparison of the Organic Flash Cycle (OFC) to Other Advanced Vapor Cycles for Intermediate and High Temperature Waste Heat Reclamation and Solar Thermal Energy. *Energy* **2012**, *42*, 213–223. [CrossRef]
50. Mondal, S.; De, S. Waste Heat Recovery through Organic Flash Cycle (OFC) Using R245fa–R600 Mixture as the Working Fluid. *Clean Technol. Environ. Policy* **2019**, *21*, 1575–1586. [CrossRef]
51. Nemati, A.; Nami, H.; Yari, M. Assessment of Different Configurations of Solar Energy Driven Organic Flash Cycles (OFCs) via Exergy and Exergoeconomic Methodologies. *Renew. Energy* **2018**, *115*, 1231–1248. [CrossRef]
52. Bonolo de Campos, G.; Bringhenti, C.; Traverso, A.; Takachi Tomita, J. Thermoeconomic Comparison between the Organic Flash Cycle and the Novel Organic Rankine Flash Cycle (ORFC). *Energy Convers. Manag.* **2020**, *215*, 112926. [CrossRef]
53. Wang, Q.; Macián-Juan, R.; Li, D. Analysis and Assessment of a Novel Organic Flash Rankine Cycle (OFRC) System for Low-Temperature Heat Recovery. *Energy Sci. Eng.* **2022**, *10*, 3023–3043. [CrossRef]
54. Wu, C.; Wang, S.; Li, J. Exergoeconomic Analysis and Optimization of a Combined Supercritical Carbon Dioxide Recompression Brayton/Organic Flash Cycle for Nuclear Power Plants. *Energy Convers. Manag.* **2018**, *171*, 936–952. [CrossRef]
55. Seyed Mahmoudi, S.M.; Ghiami Sardroud, R.; Sadeghi, M.; Rosen, M.A. Integration of Supercritical CO2 Recompression Brayton Cycle with Organic Rankine/Flash and Kalina Cycles: Thermoeconomic Comparison. *Sustainability* **2022**, *14*, 8769. [CrossRef]
56. Que, Y.; Hu, Z.; Ren, S.; Jiang, Z. Thermodynamic Analysis of a Combined Recompression Supercritical Carbon Dioxide Brayton Cycle With an Organic Flash Cycle for Hybrid Solar-Geothermal Energies Power Generation. *Front. Energy Res.* **2022**, *10*, 924134. [CrossRef]
57. Ai, T.; Chen, H.; Jia, J.; Song, Y.; Zhong, F.; Yang, S.; Xue, G. Thermodynamic Analysis of a CCHP System Integrated with a Regenerative Organic Flash Cycle. *Appl. Therm. Eng.* **2022**, *202*, 117833. [CrossRef]
58. Sadeghi, M.; Chitsaz, A.; Marivani, P.; Yari, M.; Mahmoudi, S.M.S. Effects of Thermophysical and Thermochemical Recuperation on the Performance of Combined Gas Turbine and Organic Rankine Cycle Power Generation System: Thermoeconomic Comparison and Multi-Objective Optimization. *Energy* **2020**, *210*, 118551. [CrossRef]
59. Liu, B.-T.; Chien, K.-H.; Wang, C.-C. Effect of Working Fluids on Organic Rankine Cycle for Waste Heat Recovery. *Energy* **2004**, *29*, 1207–1217. [CrossRef]
60. Hajabdollahi, Z.; Hajabdollahi, F.; Tehrani, M.; Hajabdollahi, H. Thermo-Economic Environmental Optimization of Organic Rankine Cycle for Diesel Waste Heat Recovery. *Energy* **2013**, *63*, 142–151. [CrossRef]
61. Badr, O.; Probert, S.D.; O'Callaghan, P.W. Selecting a Working Fluid for a Rankine-Cycle Engine. *Appl. Energy* **1985**, *21*, 1–42. [CrossRef]
62. Lemmon, E.W.; Huber, M.L.; McLinden, M.O. *REFPROP: Reference Fluid Thermodynamic and Transport Properties*; National Institute of Standards and Technology: Gaithersburg, MD, USA, 2007.
63. Aljundi, I.H. Effect of Dry Hydrocarbons and Critical Point Temperature on the Efficiencies of Organic Rankine Cycle. *Renew. Energy* **2011**, *36*, 1196–1202. [CrossRef]

64. Malafeev, I.I.; Il'in, G.A.; Sapozhnikov, V.B. Mathematical-Experimental Assessment of Energy Efficiency of High-Temperature Heat Pump Distiller. *Chem. Pet. Eng.* **2019**, *55*, 556–561. [CrossRef]
65. Almohammadi, B.A.; Al-Zahrani, A.; Refaey, H.A.; Attia, E.-A.; Fouda, A. Energy Analysis of a Novel Solar Tri-Generation System Using Different ORC Working Fluids. *Case Stud. Therm. Eng.* **2023**, *45*, 102918. [CrossRef]
66. Bejan, A.; Tsatsaronis, G.; Moran, M.J. *Thermal Design and Optimization*; Wiley: New York, NY, USA, 1995; ISBN 9780471584674.
67. Zoghi, M.; Habibi, H.; Chitsaz, A.; Ayazpour, M. Multi-Criteria Performance Comparison between a Novel and Two Conventional Configurations of Natural Gas—Driven Combined Cycle Power Plant Based on a Hybrid Multi-Objective Optimization. *Therm. Sci. Eng. Prog.* **2020**, *19*, 100597. [CrossRef]
68. Moran, M.J.; Shapiro, H.N.; Boettner, D.D.; Bailey, M.B. *Fundamentals of Engineering Thermodynamics*; Wiley: New York, NY, USA, 2010; ISBN 9780470495902.
69. Rizk, N.; Mongia, H. Semianalytical Correlations for NOx, CO, and UHC Emissions. *J. Eng. Gas Turbines Power Trans.* **1993**, *115*, 612–619. [CrossRef]
70. Casella, F.; Maffezzoni, C. Modelling of NOx and Co Emissions of a Small Gas Turbine Unit Based on Operational Data and Neural Networks. *IFAC Proc. Vol.* **2003**, *36*, 115–120. [CrossRef]
71. Ghaebi, H.; Saidi, M.H.; Ahmadi, P. Exergoeconomic Optimization of a Trigeneration System for Heating, Cooling and Power Production Purpose Based on TRR Method and Using Evolutionary Algorithm. *Appl. Therm. Eng.* **2012**, *36*, 113–125. [CrossRef]
72. Lazzaretto, A.; Tsatsaronis, G. A General Process-Based Methodology for Exergy Costing. In Proceedings of the ASME 1996 International Mechanical Engineering Congress and Exposition, Atlanta, GA, USA, 17–22 November 2023.
73. Shokati, N.; Mohammadkhani, F.; Yari, M.; Mahmoudi, S.M.S.; Rosen, M.A. A Comparative Exergoeconomic Analysis of Waste Heat Recovery from a Gas Turbine-Modular Helium Reactor via Organic Rankine Cycles. *Sustainability* **2014**, *6*, 2474–2489. [CrossRef]
74. Ahmadi, P.; Dincer, I. Thermodynamic and Exergoenvironmental Analyses, and Multi-Objective Optimization of a Gas Turbine Power Plant. *Appl. Therm. Eng.* **2011**, *31*, 2529–2540. [CrossRef]
75. Kwon, Y.-H.; Kwak, H.-Y.; Oh, S.-D. Exergoeconomic Analysis of Gas Turbine Cogeneration Systems. *Exergy Int. J.* **2001**, *1*, 31–40. [CrossRef]
76. Ahmadi, P.; Dincer, I.; Rosen, M.A. Exergy, Exergoeconomic and Environmental Analyses and Evolutionary Algorithm Based Multi-Objective Optimization of Combined Cycle Power Plants. *Energy* **2011**, *36*, 5886–5898. [CrossRef]
77. Schultz, K.R.; Brown, L.C.; Besenbruch, G.E.; Hamilton, C.J. *Large-Scale Production of Hydrogen by Nuclear Energy for the Hydrogen Economy*; General Atomics: San Diego, CA, USA, 2003.
78. Zare, V.; Mahmoudi, S.M.S.; Yari, M. On the Exergoeconomic Assessment of Employing Kalina Cycle for GT-MHR Waste Heat Utilization. *Energy Convers. Manag.* **2015**, *90*, 364–374. [CrossRef]
79. Okoro, O.; Nie, L.; Podstawczyk, D.; Shavandi, A. Towards a Circular Economy: Sustainability Assessment of Biorefineries for Green Energy and Polyphenolic Production from Biomass. *ChemRxiv* **2022**. [CrossRef]
80. Ganjehkaviri, A.; Mohd Jaafar, M.N.; Ahmadi, P.; Barzegaravval, H. Modelling and Optimization of Combined Cycle Power Plant Based on Exergoeconomic and Environmental Analyses. *Appl. Therm. Eng.* **2014**, *67*, 566–578. [CrossRef]
81. Cao, Y.; Zoghi, M.; Habibi, H.; Raise, A. Waste Heat Recovery of a Combined Solid Oxide Fuel Cell—Gas Turbine System for Multi-Generation Purposes. *Appl. Therm. Eng.* **2021**, *198*, 117463. [CrossRef]
82. Javaherian, A.; Yari, M.; Gholamian, E.; Carton, J.G.; Mehr, A.S. Proposal and Comprehensive Analysis of Power and Green Hydrogen Production Using a Novel Integration of Flame-Assisted Fuel Cell System and Vanadium-Chlorine Cycle: An Application of Multi-Objective Optimization. *Energy Convers. Manag.* **2023**, *277*, 116659. [CrossRef]
83. Sadeghi, M.; Mehr, A.S.; Zar, M.; Santarelli, M. Multi-Objective Optimization of a Novel Syngas Fed SOFC Power Plant Using a Downdraft Gasifier. *Energy* **2018**, *148*, 16–31. [CrossRef]